University of California - Davis
University of Florence
University of Geneva

UCD-98-13
DFF-316-7-98
UGVA-DPT-07-1011
July, 1998

Detecting and Studying the Lightest Pseudo-Goldstone Boson at Future pp, e^+e^- and $\mu^+\mu^-$ Colliders

R. Casalbuoni[a,b1], A. Deandrea[c], S. De Curtis[b],
D. Dominici[b,d], R. Gatto[a] and J. F. Gunion[e]

[a] *Départ. de Physique Théorique, Université de Genève, CH-1211 Genève 4, Suisse*
[b] *I.N.F.N., Sezione di Firenze, I-50125 Firenze, Italia*
[c] *Centre de Physique Théorique, CNRS, Luminy F-13288 Marseille, France*
[d] *Dipartimento di Fisica Università di Firenze, I-50125 Firenze, Italia*
[e] *Department of Physics, University of California, Davis, CA 95616, USA*

Abstract

For an attractive class of dynamical symmetry breaking (technicolor) models, the lightest neutral pseudo-Nambu-Goldstone boson (P^0) contains only down-type techniquarks and charged technileptons. We discuss the prospects for discovering and studying the P^0 of such models at the Tevatron and the LHC and at future e^+e^- and $\mu^+\mu^-$ colliders. Discovery of the P^0 at the Tevatron and the LHC in the $gg \to P^0 \to \gamma\gamma$ mode should be possible over a wide range of mass. We estimate that RunI Tevatron data can already be used to exclude the P^0 in the $50-200$ GeV mass range if the number of technicolors is large. At the LHC, a very precise measurement of $\Gamma(P^0 \to gg)B(P^0 \to \gamma\gamma)$ will be possible. Discovery of the P^0 at an e^+e^- collider via the reaction $e^+e^- \to \gamma P^0$ should be possible for an integrated luminosity of $L = 100$ fb^{-1} at $\sqrt{s} = 500$ GeV as long as m_{P^0} is not near m_Z. However, measuring the branching fractions and couplings of the P^0 with precision would require much more luminosity. In the $\gamma\gamma$ collider mode of operation at an e^+e^- collider, the $\gamma\gamma \to P^0 \to b\overline{b}$ signal should be very robust and could be measured with high statistical accuracy for a broad range of m_{P^0}. At a $\mu^+\mu^-$ collider, depending upon the luminosity available at low energies, discovery of the P^0 as an s-channel resonance (given its predicted coupling to $\mu^+\mu^-$) should prove possible via scanning, even if it has not already been detected elsewhere. Once the precise mass of the P^0 is known, operation of the $\mu^+\mu^-$ collider as a P^0 factory will typically allow precision measurements of enough observables to

[1] On leave from Dipartimento di Fisica Università di Firenze, I-50125 Firenze, Italia

determine the number of technicolors of the theory and (up to a discrete set of ambiguities) the fundamental parameters of the low-energy effective Lagrangian describing the Yukawa couplings of the P^0.

1 Introduction

Theories of the electroweak interactions based on dynamical symmetry breaking (DSB) avoid the introduction of fundamental scalar fields but generally predict many pseudo-Nambu-Goldstone bosons (PNGB's) due to the breaking of a large initial global symmetry group G. While observation of any of the states predicted by DSB would be exciting, it is the PNGB's that are most directly related to the DSB mechanism. Further, since they do not acquire mass from the technicolor interactions, the PNGB's are almost certainly the lightest of the new states in the physical spectrum predicted by DSB. Among the PNGB's, the colorless neutral states are unique in that they remain massless even after the interactions of the color and electroweak gauge bosons are turned on. In technicolor models, their masses derive entirely from effective four technifermion operators involving two technileptons and two techniquarks. Such operators arise from two sources: the one-loop effective potential generated from the low-energy effective Lagrangian that describes the PNGB's and their interactions with quarks and leptons; and explicit extended-technicolor gauge boson (technileptoquark) exchanges that change a techniquark into a technilepton. The one-loop contributions to the mass-squared matrix for the PNGB's exhibit an underlying $SU(2)_L \times SU(2)_R$ symmetry. The technileptoquark gauge boson exchange contributions automatically preserve this symmetry. When this symmetry is present, the lightest PNGB, denoted P^0, will contain only down-type techniquarks (and charged technileptons) and, in particular, no up-type techniquarks. As a result, its mass scale is most naturally determined by the b-quark mass and not the t-quark mass (which will set the mass of the next lightest state). Consequently, it is likely to be much lighter than all the other PNGB's. It is the phenomenology of such a P^0 that we shall focus on.

Remarkably, direct observation of a PNGB would not have been possible at any existing accelerator, however light the PNGB's are, unless the number of technicolors is very large. Further, indirect constraints, *e.g.* from precision electroweak data, are model-dependent and not particularly robust when the number of technicolors is not large. Thus, it is important to understand whether future accelerators will allow us to detect and study the PNGB's of the DSB model. It is particularly interesting to assess prospects for detecting and studying the P^0, not just because it is much the lightest state, but also because a determination of its couplings to Standard Model particles would reveal a great deal about the technicolor model even if none of the heavier PNGB's and other states are seen.

Detection of the PNGB's at the Tevatron and LHC colliders, has been extensively considered in Refs. [1, 2, 3, 4, 5, 6, 7, 8]. A convenient review is that of Ref. [5]. For the production modes studied in the above references, the net result is that PNGB discovery would not be certain, and, even if a PNGB were discovered at the Tevatron or LHC, a detailed study of its properties would be very challenging. However, inclusive gg fusion production of a neutral PNGB, followed by its decay to $\gamma\gamma$, was not given detailed consideration in the earlier work. We find that this mode holds considerable promise for P^0 discovery at the Tevatron and will almost certainly allow detection of the P^0 at the LHC. At the LHC, a precise measurement of the product of the P^0's gg partial width times its branching fraction to $\gamma\gamma$ would typically be possible. This measurement would play a pivotal role in a direct experimental determination of key parameters of the DSB model.

Detection of PNGB's at lepton colliders has also been considered. A useful treatment, in the context of a multi-scale walking technicolor model, is that of Ref. [9]. Here, we thoroughly survey the role that e^+e^- and $\mu^+\mu^-$ colliders can be expected to play in the discovery and study of the P^0. Indeed, in the type of DSB model we consider the P^0 might be the only state that is light enough to be produced at a $\sqrt{s} \leq 500$ GeV first generation e^+e^- or $\mu^+\mu^-$ collider. The most important production process for the P^0 at an e^+e^- collider is $e^+e^- \to \gamma P^0$. In the $\gamma\gamma$ collider mode of operation, one searches for $\gamma\gamma \to P^0$. The $\gamma\gamma P^0$ coupling required in these two cases arises from an anomalous vertex graph. At a $\mu^+\mu^-$ collider, one has the unique ability to s-channel produce the P^0 ($\mu^+\mu^- \to P^0$) since it has a Yukawa-like coupling to muons. We find that discovery of the P^0 in $e^+e^- \to \gamma P^0$ will be possible and that the $\gamma\gamma$ collider and $\mu^+\mu^-$ collider will provide very robust P^0 signals allowing for fairly precise measurements of rates in a variety of channels. The relative rates allow a determination of the relative strengths of different couplings of the P^0. Finally, a measurement of the P^0's total width would be possible (by scanning in the s-channel) at a $\mu^+\mu^-$ collider. The total width is the crucial ingredient needed to convert measured production rates into absolute magnitudes for the parameters of the effective Lagrangian.

It is useful to expand somewhat upon the theoretical context for our study of PNGB's. For recent reviews see Refs. [10, 11]. The idea of dynamical breaking of electroweak symmetry based on a new strong interaction goes back to Weinberg and to Susskind [12]. The original idea of a scaled-up QCD (technicolor) was extensively developed (see for instance the review by Farhi and Susskind [13]). These and many related ideas usually face substantial difficulties when attempting to construct a realistic scenario. First of all, quark and lepton masses demand additional interactions (such as extended technicolor). Apart from finding a simple solution for the heaviness of the top quark (see, for instance, the recent proposal of top-color assisted technicolor [14]), the difficulty in solving the problem of flavor changing neutral currents (FCNC) blocked concrete progress for many years.

These difficulties eventually led to the realization that the W and Z masses depend on different regions of momenta than do the quark and lepton masses. As a result, it is possible to construct theories which yield enhanced contributions in the high momentum region, without giving rise to strong effects at low momenta. In this way, it is possible to simultaneously explain the magnitudes of the intermediate vector boson masses and of the quark and lepton masses without encountering severe FCNC problems. In this context, it is important to note that PNGB masses are expected to arise from the momentum region important for quark and lepton masses. These ideas have been developed into schemes such as walking technicolor [15, 16, 17].

Another possible difficulty for technicolor models is the S parameter of electroweak precision measurements [18]. However, it has been pointed out [19] that the pseudo-Nambu-Goldstone boson loops can give negative contributions to S that can cancel the positive contributions coming from the technicolor hadrons. For example, Ref. [20] presents a specific model that incorporates such cancellations, walking technicolor, and other effects in order to obtain a value of S that is consistent with observation. We will not consider precision electroweak constraints in our analyzes other than to focus on moderate values for the number of technicolors, for which problems with S are least likely to be severe.

In this paper, the DSB model will be largely specified by a low-energy effective theory characterized by a large initial chiral symmetry group, its subgroup after spontaneous breaking, and the known local electroweak and color group. The effective low-energy Lagrangian of the theory contains a Yukawa coupling component that plays two crucial roles. First, it determines the most general form of the couplings of all the PNGB's, in particular those of the P^0, to SM fermions. Second, the one-loop potential computed from the low-energy effective Yukawa couplings gives contributions to the mass-squared matrix of the PNGB's. The relative size of these one-loop contributions to the mass-squared matrix as compared to the contributions from technileptoquark gauge boson exchange diagrams is model-dependent. However, should the one-loop contributions be dominant, the P^0 mass would then be mostly determined by the same mechanism that is responsible for the quark and lepton masses.

In the context of the low-energy effective theory there are two important scales: the effective cut-off scale Λ and the scale v related to electroweak symmetry breaking. The overall magnitude of the one-loop contributions to PNGB masses is determined by $\Lambda m_f/v$ and fermionic couplings are proportional to m_f/v (where f denotes the relevant fermion type). Typically, discovery of the P^0 (and other PNGB's) is easier for small v so long as the mass does not become so large as to push the discovery channels close to their kinematic limits. The largest possible value of v is the standard $v = 246$ GeV. This choice is that appropriate in the simplest technicolor models. In multi-scale walking technicolor models, the effective value of v for some of the PNGB's is typically 1/2 or 1/4 as large. For fixed PNGB masses, the smaller v's would imply production rates that are as much as an order of magnitude larger than for $v = 246$ GeV; detection of the PNGB's becomes much easier. For instance, the optimistic conclusions of Ref. [9] depend crucially on the presence of such enhancements in the multi-scale model they employ. We will adopt the most conservative choice of $v = 246$ GeV in our studies. Nonetheless, we find that discovery and detailed study of the P^0 should certainly be possible at future colliders. In large measure, this is due to the down-type techniquark (and technilepton) nature of the P^0, in the class of DSB model we consider, which has two important implications: (1) it guarantees that $m_{P^0}(\mathrm{one-loop}) \sim \Lambda m_b/v$ will be small (for $\Lambda \lesssim 10$ TeV); and (2) it leads to large numerical values for both the $\gamma\gamma P^0$ anomalous coupling itself and the product of the $\gamma\gamma P^0$ and ggP^0 anomalous couplings.

The outline of the paper is as follows. In Section 2, we present details of the low-energy effective Lagrangian describing PNGB's, with gradually increasing focus on the light P^0. We also discuss technileptoquark contributions to m_{P^0}. In Section 3, we present results for the branching fractions and total width of the P^0 for a representative choice of model parameters. In Section 4, prospects for P^0 detection at the Tevatron and LHC are discussed, with particular emphasis on the $gg \to P^0 \to \gamma\gamma$ mode. In Section 5, P^0 detection at an e^+e^- collider (primarily in the $e^+e^- \to \gamma P^0$ mode) is studied. In Section 6, P^0 detection at a $\gamma\gamma$ collider is discussed. Section 7 gives detailed results for discovery and study of the P^0 via s-channel production at a $\mu^+\mu^-$ collider. In Section 8, we give the procedure for combining the Tevatron/LHC measurement of $\Gamma(P^0 \to gg)B(P^0 \to \gamma\gamma)$ with the $\gamma\gamma$-collider measurement of $\Gamma(P^0 \to \gamma\gamma)B(P^0 \to b\overline{b})$ and the muon-collider measurements of $\Gamma(P^0 \to \mu^+\mu^-)B(P^0 \to F)$ ($F = \tau^+\tau^-, b\overline{b}, gg$) and $\Gamma^{\mathrm{tot}}_{P^0}$ so as to determine: (a) the number of technicolors; and (up to a discrete set of ambiguities) (b) the parameters describing the Yukawa couplings of the P^0 and (c) a tentative value for the effective cut-off scale of the low-energy theory. A discussion of expected errors for these determinations is also presented. Our conclusions are presented in Section 9.

2 Model details and resulting PNGB mass spectrum and couplings

We begin by briefly summarizing the framework we employ for computing the one-loop contributions to the PNGB mass spectrum coming from the interactions which are responsible for the masses of the ordinary fermions [21]. We will avoid the introduction of a detailed specific fundamental theory by working with the low-energy effective theory as characterized by its chiral symmetry group G, which is broken down to a subgroup H, and by the gauge group $G_W = SU(3) \otimes SU(2)_L \otimes U(1)_Y$. The first step is to write the allowed effective Yukawa couplings between the ordinary fermions and the PNGB's. These effective Yukawa couplings can be employed independently of the underlying fundamental mechanism which gives rise to them.

The allowed couplings are those which are invariant under the gauge symmetry G_W that survives in the low-energy sector. According to the general prescription of Ref. [22], these invariant couplings are specific functions of the fermion fields and of the PNGB bound-state fields that emerge in the effective theory and transform non-linearly under G. The lowest order term in the expansion of these couplings in inverse powers of the PNGB decay constant v contains the mass terms for the ordinary fermions. This allows us to obtain a set of relations among the Yukawa couplings and the ordinary fermion masses.

In general, the number of independent Yukawa couplings exceeds the number of quark and lepton masses, so that some free parameters remain. Thus, measurements of such observables as branching fractions and production rates at high-energy accelerators will be important for determining other combinations of the Yukawa couplings. The possibilities for and typical errors in the parameter determinations will be the main focus of later sections of the paper. For now, we will discuss how the masses and fermionic couplings of the PNGB's depend upon the Yukawa coupling parameters.

Given a specific form for the Yukawa couplings, the natural tool for analyzing their influence on the vacuum orientation is the effective potential. The one-loop effective potential, including the effects of both ordinary gauge interactions and Yukawa couplings, is a major ingredient in determining the PNGB mass spectrum. The other possible contributions to the PNGB mass-squared matrix are those arising at tree-level from technileptoquark exchanges.

We will specialize to the case of a $SU(8) \times SU(8)$ chiral symmetry, spontaneously broken to the diagonal $SU(8)$ subgroup. This pattern of global symmetries is realized, for instance, in the popular technicolor model [12, 13] in which the technifermions consist of a generation (U, D, N, E) of techniquarks and technileptons, with the same quantum numbers as the corresponding ordinary fermions. The spontaneous breaking of $SU(8) \times SU(8)$ to the diagonal $SU(8)$ subgroup produces 63 Goldstone bosons. One has 7 colorless goldstones π_a, $\tilde{\pi}_a$ and π_D associated to the generators T^a, $\tilde{T}^a$ and T_D $(a = 1, 2, 3)$. The states π_a are those absorbed by the W and Z via the Higgs mechanism. The states $\tilde{\pi}_3$ and π_D are the colorless, neutral states upon which we focus. In addition, there are 32 color octet goldstones: π_8^α and $\pi_8^{a\alpha}$ $(\alpha = 1, \ldots 8)$. They are related to the generators T_8^α and $T_8^{a\alpha}$. Finally, there are 24 triplet Goldstone bosons: $P_3^{\mu i}$ and $\bar{P}_3^{\mu i}$ (μ=0,1,2,3 and i=1,2,3). These are linear combinations of the fields $\pi_3^{\mu i}$ and $\bar{\pi}_3^{\mu i}$ associated with the generators $T_3^{\mu i}$ and $\bar{T}_3^{\mu i}$ (for the list of the $SU(8)$ generators see Ref. [21]).

In the single-scale technicolor model based on $SU(8) \times SU(8)$, the low-energy gauge interactions of the Goldstone bosons are described by the Lagrangian [23]

$$\mathcal{L}_g = \frac{v^2}{16} Tr \left(\mathcal{D}_\mu U^\dagger \mathcal{D}_\mu U \right) \tag{1}$$

where

$$U = \exp \left(\frac{2iT^s \pi^s}{v} \right) \tag{2}$$

with $v = 246$ GeV. The generators T^s $(s = 1, \ldots, 63)$ are normalized according to $Tr(T^r T^s) = 2\delta^{rs}$. The covariant derivative $\mathcal{D}_\mu U$ is given by

$$\mathcal{D}_\mu U = \partial_\mu U + \mathcal{A}_\mu U - U \mathcal{B}_\mu \tag{3}$$

where

$$
\begin{aligned}
\mathcal{A}_\mu &= W_\mu + \hat{B}'_\mu + G_\mu & \mathcal{B}_\mu &= \hat{B}_\mu + \hat{B}'_\mu + G_\mu \\
W_\mu &= igT^a W^a_\mu & \hat{B}_\mu &= ig' T^3 B_\mu \\
\hat{B}'_\mu &= ig' \frac{T_D}{\sqrt{3}} B_\mu & G_\mu &= i\frac{g_s}{\sqrt{2}} T^\alpha_8 G^\alpha_\mu
\end{aligned} \tag{4}
$$

In Eq. (4), W^a_μ ($a = 1, 2, 3$), B_μ and G^α_μ ($\alpha = 1, \cdots, 8$), are the gauge vector fields related to the gauge group G_W.

In a multi-scale technicolor model, the above would be generalized by writing $\mathcal{L}_g$ as a sum of terms involving different v_i's, where each term would contain a U_i that depends on a subset of the π^s fields. (Such a structure would amount to an explicit breaking of the $SU(8) \times SU(8)$ symmetry by $\mathcal{L}_g$.) By requiring $\sum_i v_i^2 = v^2 = (246\text{ GeV})^2$, correct values for the W and Z masses are obtained, and, if each U_i has $1/v_i$ in the exponent, the kinetic energy terms for the π's that are in the exponent will be correctly normalized. The term of relevance for our purposes would be that which contains the neutral color-singlet π_D and $\tilde{\pi}_3$ isosinglet and isotriplet fields. As regards these fields, the discussion to be presented would then be unaltered except that the value of v would be replaced by a smaller value (typically $v/2$ or $v/4$).

In order to write the Yukawa couplings between the Goldstone bosons and the ordinary fermions we decompose the matrix U according to

$$
U = \begin{pmatrix}
U^{ij}_{uu} & U^{ij}_{ud} & U^k_{u\nu} & U^k_{ue} \\
U^{ij}_{du} & U^{ij}_{dd} & U^k_{d\nu} & U^k_{de} \\
U^l_{\nu u} & U^l_{\nu d} & U_{\nu\nu} & U_{\nu e} \\
U^l_{eu} & U^l_{ed} & U_{e\nu} & U_{ee}
\end{pmatrix} \tag{5}
$$

The indices i, j, k and l are color indices running from 1 to 3. The most general Yukawa coupling invariant with respect to G_W is given in [21]. With the exception of the coupling to muons (as needed for the $\mu^+\mu^-$ collider study), only the couplings involving the third family are phenomenologically relevant for accelerator physics. (This is because, as usual, the magnitudes of the Yukawa couplings are most naturally set by the scale of the corresponding fermionic masses.) It is only these Yukawa couplings that we can hope to determine. Thus, we consider the effective Yukawa coupling Lagrangian

$$
\begin{aligned}
\mathcal{L}_Y = &- m_1 \left(\bar{t}^i_R U^{\dagger ij}_{uu} t^j_L + \bar{t}^i_R U^{\dagger ij}_{du} b^j_L + h.c.\right) \\
&- m_2 \left(\bar{b}^i_R U^{\dagger ij}_{ud} t^j_L + \bar{b}^i_R U^{\dagger ij}_{dd} b^j_L + h.c.\right) \\
&- m_4 \left(\bar{\tau}_R U^\dagger_{\nu e} \nu_{\tau L} + \bar{\tau}_R U^\dagger_{ee} \tau_L + h.c.\right) \\
&- m_4^{(2)} \left(\bar{\mu}_R U^\dagger_{\nu e} \nu_{\mu L} + \bar{\mu}_R U^\dagger_{ee} \mu_L + h.c.\right) \\
&- m_5 \left(\bar{t}^i_R U^{\dagger jj}_{uu} t^i_L + \bar{t}^i_R U^{\dagger jj}_{du} b^i_L + h.c.\right) \\
&- m_6 \left(\bar{b}^i_R U^{\dagger jj}_{ud} t^i_L + \bar{b}^i_R U^{\dagger jj}_{dd} b^i_L + h.c.\right) \\
&- m_7 \left(\bar{t}^i_R U^\dagger_{\nu\nu} t^i_L + \bar{t}^i_R U^\dagger_{e\nu} b^i_L + h.c.\right)
\end{aligned}
$$

$$
\begin{aligned}
&- m_9 \left(\bar{b}^i_R U^\dagger_{\nu e} t^i_L + \bar{b}^i_R U^\dagger_{ee} b^i_L + h.c.\right) \\
&- m_{10} \left(\bar{\tau}_R U^{\dagger jj}_{ud} \nu_{\tau L} + \bar{\tau}_R U^{\dagger jj}_{dd} \tau_L + h.c.\right) \\
&- m^{(2)}_{10} \left(\bar{\mu}_R U^{\dagger jj}_{ud} \nu_{\mu L} + \bar{\mu}_R U^{\dagger jj}_{dd} \mu_L + h.c.\right) \\
&- m_{11} \left[\bar{t}_R \lambda^\alpha \left(\begin{array}{cc} U^\dagger_{uu} & U^\dagger_{du} \end{array} \right) \left(\begin{array}{cc} \lambda^\alpha & 0 \\ 0 & \lambda^\alpha \end{array} \right) \left(\begin{array}{c} t_L \\ b_L \end{array} \right) + h.c.\right] \\
&- m_{12} \left[\bar{b}_R \lambda^\alpha \left(\begin{array}{cc} U^\dagger_{ud} & U^\dagger_{dd} \end{array} \right) \left(\begin{array}{cc} \lambda^\alpha & 0 \\ 0 & \lambda^\alpha \end{array} \right) \left(\begin{array}{c} t_L \\ b_L \end{array} \right) + h.c.\right] . \qquad (6)
\end{aligned}
$$

In the above, we have omitted terms involving only colored PNGB's, and kept only couplings for the third family, with the exception of the parameters $m^{(2)}_{4,10}$ which determine the PNGB couplings to muons. In Eq. (6), we have also assumed no generation-mixing terms, thereby automatically guaranteeing absence of flavor-changing neutral current interactions. For later reference, it is useful to note that in the (U, D, N, E) realization of our model, the U_{uu}, U_{dd}, $U_{\nu\nu}$ and U_{ee} entries above come from techni-U, D, N and E fermion propagator loop corrections, respectively.

It will be important to understand how the (two) neutral color-singlet PNGB states enter in the notation of Eq. (6). For this purpose we define the states

$$
P^0 = \frac{\tilde{\pi}_3 - \pi_D}{\sqrt{2}} , \qquad P^{0\prime} = \frac{\tilde{\pi}_3 + \pi_D}{\sqrt{2}} , \qquad (7)
$$

which, as discussed shortly, are the mass eigenstates in the class of models we consider. Expanding to first order in $1/v$, we have

$$
\begin{aligned}
U^{ij}_{uu} &\sim \delta^{ij} \left[1 + \frac{i}{v}\sqrt{6}\frac{P^{0\prime}}{3}\right] + \ldots \\
U^{ij}_{dd} &\sim \delta^{ij} \left[1 - \frac{i}{v}\sqrt{6}\frac{P^{0}}{3}\right] + \ldots \\
U_{\nu\nu} &\sim \left[1 - \frac{i}{v}\sqrt{6}P^{0\prime}\right] + \ldots \\
U_{ee} &\sim \left[1 + \frac{i}{v}\sqrt{6}P^{0}\right] + \ldots . \qquad (8)
\end{aligned}
$$

Non-neutral entries (U^{ij}_{ud}, $U_{\nu e}$ *etc.*) contain neither $\mathcal{O}(1)$ terms nor neutral P^0 and $P^{0\prime}$ fields (but, rather, contain charged PNGB's) in their $1/v$ expansion. We note that this expansion assumes that we begin with the correct vacuum state, implying that the masses of the PNGB fields appearing in the U_{ij}'s must all be positive. This will imply constraints on the m_i parameters of Eq. (6).

From the $\mathcal{O}(1)$ terms in the expansion of $\mathcal{L}_Y$ we easily recover the expressions for the fermion masses

$$
\begin{aligned}
m_t &= m'_1 + m_7 \\
m_b &= m'_2 + m_9
\end{aligned}
$$

$$
\begin{aligned}
m_\tau &= m_4 + 3m_{10} \\
m_\mu &= m_4^{(2)} + 3m_{10}^{(2)} \\
m_{\nu_\tau} &= m_{\nu_\mu} = 0\,,
\end{aligned} \tag{9}
$$

where

$$
m_1' \equiv m_1 + 3m_5 + \frac{16}{3}m_{11}\,, \quad m_2' \equiv m_2 + 3m_6 + \frac{16}{3}m_{12}\,. \tag{10}
$$

Note that the fermion masses provide 4 constraints on the independent parameters appearing in $\mathcal{L}_Y$.

We note that in the multi-scale case, it is precisely the U_i that contains the color-singlet neutral P^0 and $P^{0\prime}$ that will be responsible for fermion masses and that would appear in Eq. (6). This means that the $1/v$ that appears in the expansions of Eq. (8) would be replaced by $1/v_i$. This $1/v_i$ factor would then emerge in the Yukawa couplings and mass contributions for the P^0 to be discussed below.

Starting from the interaction Lagrangian $\mathcal{L}_g + \mathcal{L}_Y$, the next step is to evaluate the one-loop effective potential. Let us assume for the moment that it is the only contribution to the PNGB mass-squared matrix. Then, all PNGB masses would be obtained by its diagonalization as detailed in [21]. In particular, we will focus on the neutral color-singlet PNGB's. The mass matrix in the P^0–$P^{0\prime}$ basis arises from one-loop diagrams involving the quark and lepton fields to which they couple, where the momenta of the loops are integrated up to scale Λ. Using Eq. (6), one finds that the P^0 and $P^{0\prime}$ are, in fact, mass eigenstates and that the one-loop contributions to their masses-squared are given by:

$$
m^2_{P^0}(\mathrm{one-loop}) = \frac{4\Lambda^2}{\pi^2 v^2}\rho_8\,, \quad m^2_{P^{0\prime}}(\mathrm{one-loop}) = \frac{4\Lambda^2}{\pi^2 v^2}\rho_7\,, \tag{11}
$$

where

$$
\rho_8 = 2m_2' m_9 + 2m_4 m_{10} + 2m_4^{(2)} m_{10}^{(2)}\,, \quad \rho_7 = 2m_1' m_7 \tag{12}
$$

and Λ is the UV cut-off, situated in the TeV region. Notice that, as promised, P^0 and $P^{0\prime}$ receive no mass contributions from the gauge interactions in (1). Further, the P^0 mass arises only from the terms involving b, τ and μ in $\mathcal{L}_Y$ while the $P^{0\prime}$ mass arises from terms involving the t. Terms proportional to m_i^2 (*e.g.* $m_2'^2$, m_9^2, … contributions to $m^2_{P^0}$) are absent due to the cancellation between the standard self-energy bubble diagrams resulting from the 'square' of $\mathcal{O}\,(1/v)$ terms in the expansion of the U fields appearing in $\mathcal{L}_Y$, as given by using Eq. (8), and diagrams arising from the quadratic couplings that first appear at order $\mathcal{O}\,(1/v^2)$ in the expansion of the U fields in $\mathcal{L}_Y$.

A useful point of reference for this discussion is the one-family technicolor scheme of Refs. [12, 13]. There, the $\tilde{\pi}_3$ and π_D states are given in terms of the (U, D, N, E) techniquarks and technileptons as:

$$
\tilde{\pi}_3 = \frac{1}{\sqrt{24}}(U\overline{U} - D\overline{D} - 3N\overline{N} + 3E\overline{E})\,, \tag{13}
$$

$$
\pi_D = \frac{1}{\sqrt{24}}(U\overline{U} + D\overline{D} - 3N\overline{N} - 3E\overline{E})\,, \tag{14}
$$

where there is an implicit color summation in the $U\overline{U}$ and $D\overline{D}$ combinations. The P^0 and $P^{0\prime}$ mass eigenstates of Eq. (7) then take the forms:

$$P^0 = \frac{1}{\sqrt{12}}(3E\overline{E} - D\overline{D})\,, \tag{15}$$

$$P^{0\prime} = \frac{1}{\sqrt{12}}(U\overline{U} - 3N\overline{N})\,, \tag{16}$$

which are purely $T_3 = -1/2$ and $T_3 = +1/2$ isospin states, respectively. Contributions to the π_D–$\tilde{\pi}_3$ mass-squared matrix come from four-technifermion operators in the low-energy effective theory that fail to commute with the currents to which π_D and $\tilde{\pi}_3$ couple. The only operators that fail to commute with the π_D and $\tilde{\pi}_3$ currents are ones involving two techniquarks and two technileptons (see, for example, Refs. [2] and [13]). For instance, the combination $D\overline{D}E\overline{E}$ will give mass to the P^0. This explains the absence of squared masses in the expressions for ρ_8 and ρ_7 discussed in the previous paragraph. Since Yukawa coupling contributions to PNGB masses must come from effective four-technifermion operators that contain two techniquark and two technilepton fields, only $m_f m_{f'}$ cross terms can contribute. Thus, for example, the $m_2 m_9$ term comes from a U_{dd}–U_{ee} cross term that creates via a b-quark loop a $\langle D\overline{D}E\overline{E}\rangle$ effective four-technifermion interaction.

We emphasize that it is the P^0 and $P^{0\prime}$ that are mass eigenstates of the one-loop effective potential and not the π_D and $\tilde{\pi}_3$ (isosinglet and isotriplet) states. This can be understood as being due to the fact that the underlying $SU(2)_L \times SU(2)_R$ invariance of the techniquark and technilepton sector of the theory remains unbroken in the chiral limit (see also [24]). This implies that the m^2 operator that breaks the chiral symmetry must commute with the charge operator $T_3 \equiv T_{3L} + T_{3R}$ and, therefore, take the form

$$m^2 = A\mathbf{1} + BK_3 + CT_3 \tag{17}$$

where $K_3 \equiv T_{3L} - T_{3R}$ (which implicitly contains a $-\gamma_5$) is the only matrix other than the unit matrix and T_3 itself that commutes with T_3.[2] In the $\tilde{\pi}_3$–π_D basis, m^2 then necessarily takes the form $m^2 = \begin{pmatrix} A & B \\ B & A \end{pmatrix}$, which is diagonalized in the P^0–$P^{0\prime}$ basis with eigenvalues $A - B$ and $A + B$, respectively. As discussed shortly, the $SU(2)_L \times SU(2)_R$ symmetry is preserved by the other possibly important contributions to the mass-squared matrix, so that P^0 will, indeed, be a mass eigenstate. This important result leads to significant differences in the phenomenology of the P^0 as compared to what would be the case for $\tilde{\pi}_3$ and π_D being mass eigenstates.

[2]The generality of this mass matrix is most easily derived in the P^0–$P^{0\prime}$ basis. From the requirement that m^2 and Q commute, m^2 must depend only on T_{3L} and T_{3R}. The P^0 and $P^{0\prime}$ belong to the representation (1/2,1/2) of $SU(2)_L \times SU(2)_R$. Therefore, for them, $T_{3L}^2 = T_{3R}^2 = -T_{3L}T_{3R} = 1/4$ (where, for the last equality remember that $T_{3L} + T_{3R} = 0$ for the neutral states of interest). Therefore, one needs to keep only linear terms in T_{3L} and T_{3R} in m^2.

In the (U, D, N, E) one-family model, the meaning of A and B of Eq. (17) becomes very apparent. One finds

$$A = m_{D,E}^2 + m_{U,N}^2 \,, \qquad B = m_{U,N}^2 - m_{D,E}^2 \,, \tag{18}$$

where $m_{U,N}^2$ is the contribution coming from $\langle U\overline{U}\rangle\langle N\overline{N}\rangle$ and $m_{D,E}^2$ is the contribution from $\langle D\overline{D}\rangle\langle E\overline{E}\rangle$. After diagonalization, one then finds

$$m_{P^0}^2 = 2m_{D,E}^2 \,, \qquad m_{P^{0\prime}}^2 = 2m_{U,N}^2 \,. \tag{19}$$

Since, in this model, $\langle D\overline{D}\rangle$ and $\langle E\overline{E}\rangle$ determine m_b, while $\langle U\overline{U}\rangle$ and $\langle N\overline{N}\rangle$ determine m_t, $m_{P^0} \ll m_{P^{0\prime}}$, as implicit in Eqs. (9), (11) and (12), is a very natural expectation.

Let us now go consider the possible four-technifermion operator contributions to the π_D–$\tilde{\pi}_3$ mass-squared matrix in more generality. In fact, there are only two important sources of such operators. The first is the one-loop effective potential, as discussed above, where the masses-squared for the P^0 and $P^{0\prime}$ were explicitly noted to have come from operators induced by SM quark and lepton loops that mixed techniquark and technilepton bilinears. These derive from the one-loop diagrams constructed from tree-level exchanges of the extended technicolor (ETC) gauge bosons that mediate (U, D, N, E) to (t, b, ν, τ) transitions. The second contribution is that from heavy technileptoquark (LQ) gauge boson exchange at tree-level, where the LQ gauge bosons are those mediating $N \to U$ and $E \to D$ transitions in (U, D, N, E) techni-flavor space.[3] These ETC and LQ gauge bosons are intimately connected by the generator algebra

$$[Q_L^a, Q_L^b] = if^{abc}Q_L^c \,, \quad [Q_R^a, Q_R^b] = if^{abc}Q_R^c \,, \quad [Q_R^a, Q_L^b] = 0 \,, \tag{20}$$

and related current algebra, where if, for example, a and b are chosen to give ETC $E \to b$ and $b \to D$ transitions, respectively, then f^{abc} will be non-zero for the LQ $E \to D$ transition. This means that if ETC gauge bosons are present then the group structure demands that the LQ gauge bosons also be present. Further, they must have chiral structure correlated with that of the ETC gauge bosons. Using the notation $g_{\rm LQ}^L$ and $g_{\rm LQ}^R$ for the coefficients[4] defining the left-handed and right-handed components of the LQ gauge boson currents, with similar definitions for the ETC gauge boson currents, Eq. (20) requires $g_{\rm LQ}^{R,L} = [g_{\rm ETC}^{R,L}]^2$.

Explicit computation of the LQ extended-technicolor gauge boson exchanges (following the techniques of Ref. [2]) yields the result that the LQ contributions to the π_D–$\tilde{\pi}_3$ mass-squared matrix take the same form as given in Eqs. (17), (18) and

[3]These latter can be thought of as being a subset of Pati-Salam-like $SU(4)$ group gauge bosons operating in the $(U_{1,2,3}, N)$ and $(D_{1,2,3}, E)$ subspaces (where we have exposed the color indices $1, 2, 3$).

[4]These $g^{R,L}$ do not include the overall gauge coupling constant, g.

(19). This result obtains for any relative weight of $g^L_{\rm LQ}$ vs. $g^R_{\rm LQ}$. Explicitly, the LQ contributions would contribute (see Refs. [2] and [13])

$$m^2_{D,E}({\rm LQ}) \sim g^2 \frac{g^L_{\rm LQ} g^R_{\rm LQ}}{m^2_{\rm LQ}} \frac{\langle D\overline{D}\rangle\langle E\overline{E}\rangle}{F_T^2}\,, \tag{21}$$

to $m^2_{P^0}$, with a similar contribution to $m^2_{P^{0\prime}}$ proportional to $\langle U\overline{U}\rangle\langle N\overline{N}\rangle$. (Here, $m_{\rm LQ}$ specifies the mass of the relevant technileptoquark type Pati-Salam gauge bosons and F_T represents the effective technipion decay constant.) Thus, even after including LQ exchanges, the P^0 and $P^{0\prime}$ are the mass eigenstates. And, once again, the appearance of $\langle D\overline{D}\rangle\langle E\overline{E}\rangle$ in $m^2_{D,E}$ and of $\langle U\overline{U}\rangle\langle N\overline{N}\rangle$ in $m^2_{U,N}$ guarantees that the m_{P^0} and $m_{P^{0\prime}}$ are most naturally related to the m_b and m_t SM-fermion masses, respectively. Because of the possibility that LQ mass-squared contributions are significant, our phenomenological studies will not assume a specific relation between the mass of the P^0 and its Yukawa coupling parameters. That the mass eigenstate is the P^0 as defined in Eqs. (7) and (15) will, however, be quite important for the phenomenology.

A natural question is whether or not it is possible for the one-loop mass-squared matrix contributions to dominate over the LQ contributions. This would produce a very self-contained theory with all masses as well as couplings determined by the one-loop effective potential. We need to compare the result of Eq. (21) to the one-loop effective potential terms. In our notation, the latter are of order $\Lambda^2 m_f m_{f'}/\pi^2 F_T^2$ (where we have used $v \sim 2F_T$, as appropriate for this model). Using the fact that $m_f \sim \langle F\overline{F}\rangle g^2 g^L_{\rm ETC} g^R_{\rm ETC}/m^2_{\rm ETC}$, where F is the technifermion coupled to f by the ETC gauge boson, and writing $\Lambda \equiv \lambda m_{\rm ETC}$, the one-loop effective potential contributes, for example,

$$m^2_{D,E}({\rm ETC}) \sim \frac{\lambda^2 g^4 [g^L_{\rm ETC} g^R_{\rm ETC}]^2}{m^2_{\rm ETC}} \frac{\langle D\overline{D}\rangle\langle E\overline{E}\rangle}{\pi^2 F_T^2}\,. \tag{22}$$

In comparing Eq. (22) to Eq. (21), we first recall that $g^{R,L}_{\rm LQ} = [g^{R,L}_{\rm ETC}]^2$, implying exactly the same chiral structure for the two contributions. In particular, one cannot have $m^2(LQ) \to 0$ as a result of $g^L_{\rm LQ} \to 0$ or $g^R_{\rm LQ} \to 0$ without killing the one-loop $m^2({\rm ETC})$ contribution at the same rate. Further, one cannot take $m_{\rm LQ} \gg m_{\rm ETC}$ since the ETC gauge bosons cannot form a subgroup on their own without inclusion of the LQ gauge bosons; most naturally, $m_{\rm LQ} \sim m_{\rm ETC}$. Only if the product $\lambda^2 g^2/\pi^2$ is very large could the one-loop mass contributions dominate over the LQ mass contributions. Now, λ^2 implicitly contains the usual one-loop $C_{\rm ETC}/16$ factor, where $C_{\rm ETC}$ could be computed for a given ETC group for the two-ETC-gauge-boson exchange diagram underlying Eq. (22). Writing $\lambda^2 \equiv \kappa^2 C_{\rm ETC}/16$, $\alpha_{\rm ETC} \equiv g^2/4\pi$, and taking $C_{\rm ETC}/4 \sim 1$ (a not atypical value), we would need to have $\kappa^2 \alpha_{\rm ETC}/\pi \gg 1$ for one-loop dominance. If the one-loop ETC contributions to the mass-squared matrix dominate, Eq. (11) could then be used to determine Λ from the measured value of m_{P^0} once all the parameters in ρ_8 of Eq. (12) have been determined from experiment. The determination of Λ made assuming dominance of the one-loop ETC diagrams can be expected to at least provide a rough idea (*i.e.* to within a factor of 3 or 4, see below) of the ETC gauge boson scale.

What is a natural expectation for λ and thence $\kappa^2\alpha_{\rm ETC}/\pi$? In QCD chiral theory, the analogue of λ is $4\pi f_\pi/\Lambda_{\rm QCD} \sim$ [1.2 GeV/300 MeV] ~ 4 [25, 26]; the corresponding $\kappa^2\alpha_s/\pi$ is then of order $\sim [4]^2 \times 4\alpha_s/\pi$, which would, indeed, be much larger than 1. Another example is provided by the Fermi theory, where the natural cutoff is about 300 GeV (the unitarity limit), whereas the mass of the mediating gauge bosons is about 100 GeV, corresponding to $\lambda \sim 3$. Generally speaking, the cut-off scale at which the effective theory breaks down is significantly larger than the typical mass of the underlying exchanged gauge boson(s). The only exception arises if there is additional new physics at scales just above the gauge boson mass scale. There is no requirement in the context of ETC that this be the case, although it cannot be ruled out. Thus, we believe it is quite possible that the one-loop mass contributions could dominate $m^2_{P^0}$, in which case the physics of the P^0 would be entirely determined by the effective Lagrangian and a determination of Λ would be possible.

Let us now turn to the couplings of the P^0 to SM particles. By inserting the expansion to first order in the PNGB fields given in Eq. (8) into Eq. (6), we easily obtain the couplings of the P^0 and $P^{0\prime}$ to fermions. Obviously, the P^0 boson couples to the $T_3 = -1/2$ component of the fermion doublets, while $P^{0\prime}$ couples to the $T_3 = +1/2$ component. It is the P^0 upon which we focus; its Yukawa couplings to fermions are:

$$\mathcal{L}_Y = -i\lambda_b \bar{b}\gamma_5 b P^0 - i\lambda_\tau \bar{\tau}\gamma_5 \tau P^0 - i\lambda_\mu \bar{\mu}\gamma_5 \mu P^0 \tag{23}$$

with

$$\lambda_b = -\frac{\sqrt{6}}{3v}\left(m_2' - 3m_9\right) , \quad \lambda_\tau = \frac{\sqrt{6}}{v}\left(m_4 - m_{10}\right) , \quad \lambda_\mu = \frac{\sqrt{6}}{v}\left(m_4^{(2)} - m_{10}^{(2)}\right) . \tag{24}$$

It is important to note that λ_b, m_{P^0} [Eqs. (11) and (12)], and m_b [Eq. (9)] all depend only on the combination m_2' defined in Eq. (10). Thus, the complete set of parameters describing the $T_3 = -1/2$ sector phenomenology comprises m_2', m_4, $m_4^{(2)}$, m_9, m_{10} and $m_{10}^{(2)}$, for a total of six parameters. Since the above Yukawa couplings involve different combinations of these six parameters than do the fermion masses (m_b, m_τ and m_μ), all six mass parameters can be independently determined using the known fermion mass values if experimental measurements of λ_b, λ_μ and λ_τ are available. Given a determination of the six m_i, the value of ρ_8 in Eq. (12) can be computed and the measured m_{P^0} will yield a result for Λ through Eq. (11) if the LQ contribution to $m^2_{P^0}$ is small. Clearly, our ability to measure the Yukawa couplings will be an important focus of our phenomenological discussion.

As already apparent from Eq. (9), the parameters m_i are of the order of the masses of the corresponding fermions. In order to explore a representative phenomenological case, in Ref. [27] we made the following choices:

$$\begin{aligned}
m_1' &= m_7 = \frac{m_t}{2} \\
m_2' &= m_9 = \frac{m_b}{2} \\
m_{10} &= -m_4 = \frac{m_\tau}{2} \\
m_{10}^{(2)} &= -m_4^{(2)} = \frac{m_\mu}{2} \,.
\end{aligned} \tag{25}$$

This particular set of choices is based on the assumption of no relevant cancellations. The corresponding one-loop P^0 and $P^{0\prime}$ masses are

$$m_{P^0}^2(\mathrm{one-loop}) = \frac{2\Lambda^2}{\pi^2 v^2} m_b^2 \,, \quad m_{P^{0\prime}}^2(\mathrm{one-loop}) = \frac{2\Lambda^2}{\pi^2 v^2} m_t^2 \,, \tag{26}$$

where we have neglected contributions to $m_{P^0}^2$ from the one-loop potential proportional to m_μ^2 and m_τ^2. The fermionic couplings of the P^0 corresponding to Eq. (25) are

$$\lambda_b = \sqrt{\frac{2}{3}} \frac{m_b}{v} \,, \quad \lambda_\tau = -\sqrt{6} \frac{m_\tau}{v} \,, \quad \lambda_\mu = -\sqrt{6} \frac{m_\mu}{v} \,. \tag{27}$$

More generally, we would have $\lambda_f = \xi_f m_f / v$ with ξ_f a number of the order of 1 which depends on the particular choice of the Yukawa parameters.

Our phenomenological analysis will be performed with the choice of couplings to fermions given in Eq. (27). This is a purely representative choice that will allow us to make a first assessment of the prospects for determining *directly from experiment* all those m_i parameters in $\mathcal{L}_Y$ associated with the P^0, as well as other important parameters of the model.

Also of importance are the couplings of the P^0 to a pair of SM gauge bosons arising through the ABJ anomaly [1, 2, 3, 28, 5]. These are model-dependent. We will employ those obtained in the standard technicolor theories of Ref. [1, 2, 3]. The relevant Feynman-rule (which in our notation will include double Wick contractions when two identical gauge bosons are present) for such a coupling can be written in the general form:

$$g_{PV_1V_2} = \frac{\alpha N_{TC} A_{PV_1V_2}}{\pi v} \epsilon_{\lambda\mu\nu\rho} p_1^\lambda \epsilon_1^\mu p_2^\nu \epsilon_2^\rho \,, \tag{28}$$

where for $P = P^0$ we have:

$$A_{P^0\gamma\gamma} = -\frac{4}{\sqrt{6}} \left(\frac{4}{3}\right) \tag{29}$$

$$A_{P^0 Z\gamma} = -\frac{4}{2\sqrt{6}} \left(\frac{1-4s_W^2}{4 s_W c_W} - \frac{t_W}{3}\right) \tag{30}$$

$$A_{P^0 ZZ} = -\frac{4}{\sqrt{6}} \left(\frac{1-2s_W^2}{2c_W^2} - \frac{t_W^2}{3}\right) \tag{31}$$

$$A_{P^0 gg} = \frac{1}{\sqrt{6}} \,, \tag{32}$$

where $s_W = \sin\theta_W$, *etc.* Similar results apply for the $P^{0\prime}$, but are not needed for our phenomenological studies that will be confined to the lighter P^0. We note that the couplings above are precisely those obtained in the one-family (U, D, N, E) technicolor model when F_T of the model is chosen so as to obtain correct values for m_W and m_Z: namely $F_T = v/2$ (with $v = 246$ GeV). These ABJ anomaly couplings also provide a nice illustration of the importance of knowing the mass eigenstate composition. For example, the very crucial $\gamma\gamma$ and gg couplings-squared for the P^0, π_D and $\tilde{\pi}_3$ are in the ratio $A^2_{P^0\gamma\gamma} : A^2_{\pi_D\gamma\gamma} : A^2_{\tilde{\pi}_3\gamma\gamma} = 8 : 1 : 9$ and $A^2_{P^0gg} : A^2_{\pi_Dgg} : A^2_{\tilde{\pi}_3gg} = 1 : 2 : 0$, respectively, implying very different phenomenology were the π_D or $\tilde{\pi}_3$ the lowest mass eigenstate.

We noted earlier that in the multi-scale/walking technicolor context the value of v appropriate for determining the P^0 couplings could be smaller than $v = 246$ GeV. From the above explicit formulae, it is apparent that all couplings of interest are proportional to $1/v$, implying that a decrease in v could only increase production rates for the P^0 and, thereby, our ability to discover and study the P^0 in the various channels that will be discussed later.

Finally, it is useful to consider the limit in which LQ mass-squared matrix contributions can be neglected relative to the one-loop effective potential contributions of Eq. (26). The magnitude of m_{P^0} in this limit can be better appreciated by writing the one-loop contribution to m_{P^0} from Eq. (26) in the form

$$m_{P^0}(\mathrm{one-loop}) \sim 8 \text{ GeV} \times \Lambda(\mathrm{TeV})\,. \tag{33}$$

Given that $\Lambda < 10$ TeV is most natural in the model being considered, the P^0 would be likely to have mass below m_Z. Only if Λ is unexpectedly large and/or the LQ contributions are very substantial is it possible that m_{P^0} would be larger than ~ 200 GeV.[5] In contrast, because $m_{P^{0\prime}}/m_{P^0}$ is most naturally $\propto m_t/m_b$, the $P^{0\prime}$ would be unlikely to have mass below ~ 250 GeV, and, if Λ is large and/or LQ contributions substantial, it would be a good deal heavier.

It is because the mass of the P^0 is most naturally small, in particular almost certainly much smaller than that of the $P^{0\prime}$, and because the $P^{0\prime}$ cannot be studied in the s-channel resonance mode at a muon collider (due to the fact that it does not couple to charged leptons), that we choose to focus on the phenomenology of the P^0 in this paper. We will give detailed results for $10 \leq m_{P^0} \leq 200$ GeV.

3 P^0 branching fractions and width

In this section, we give a brief summary of the branching fractions and total width of the light P^0. The P^0 Yukawa couplings to fermions are given in Eq. (27). For P^0 decays, the $\gamma\gamma$ and gluon-gluon channels are also important; the corresponding couplings are those summarized in Eqs. (29) and (32), as generated by the ABJ

[5] Walking/multi-scale technicolor models would have smaller v which would enhance the one-loop contributions to $m^2_{P^0}$ and $m^2_{P^{0\prime}}$, and could also lead to m_{P^0} values above 200 GeV.

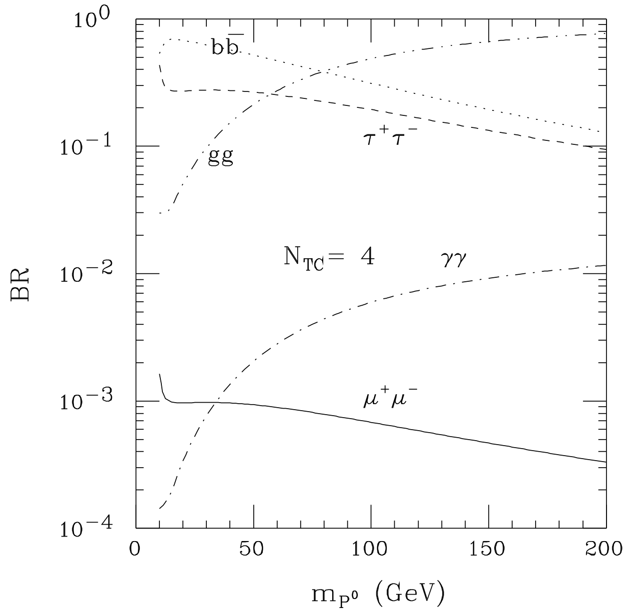

Figure 1: Branching fractions for P^0 decay into $\mu^+\mu^-$, $\tau^+\tau^-$, $b\bar{b}$, $\gamma\gamma$, and gg. We assume $N_{TC} = 4$ and employ the couplings of Eqs. (27), (29) and (32).

anomaly. The corresponding partial widths must be computed keeping in mind that, for our normalization of $A_{P^0\gamma\gamma}$ and A_{P^0gg}, one must include a factor of 1/2 for identical final state particles:

$$\Gamma(P^0 \to VV) = \frac{1}{2} C_V \frac{m_{P^0}^3}{32\pi} A_{P^0VV}^2\,, \tag{34}$$

where $C_V = 1$ (8) for $V = \gamma$ (g). We list here those partial widths relevant for our analysis:

$$\begin{aligned}
\Gamma(P^0 \to \bar{f}f) &= C_F \frac{m_{P^0}}{8\pi} \lambda_f^2 \left(1 - \frac{4m_f^2}{m_{P^0}^2}\right)^{1/2} \\
\Gamma(P^0 \to gg) &= \frac{\alpha_s^2}{48\pi^3 v^2} N_{TC}^2 m_{P^0}^3 \\
\Gamma(P^0 \to \gamma\gamma) &= \frac{2\alpha^2}{27\pi^3 v^2} N_{TC}^2 m_{P^0}^3\,,
\end{aligned} \tag{35}$$

where $C_F = 1(3)$ for leptons (down-type quarks) and N_{TC} is the number of technicolors.

The resulting branching fractions are shown in Fig. 1 and the total width is shown in Fig. 2. These results are for $N_{TC} = 4$. We see that the largest branching fractions are to $b\bar{b}$, $\tau^+\tau^-$ and gg. The total width, which is of particular relevance to muon collider phenomenology, is typically in the few MeV range, which is similar to that expected for a light SM-like Higgs boson.

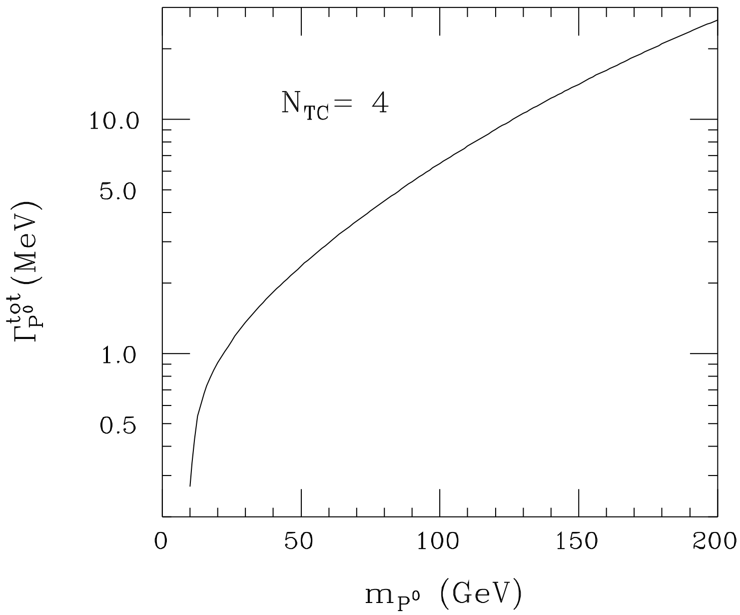

Figure 2: $\Gamma^{tot}_{P^0}$ as a function of m_{P^0}. We assume $N_{TC} = 4$ and employ the couplings of Eqs. (27), (29) (32).

There are two important features of these results that apply in the limit of large N_{TC} and/or large m_{P^0} and that are already apparent in Fig. 1: (a) the dominance of the partial width $\Gamma(P^0 \to gg)$; (b) $B(P^0 \to \gamma\gamma) \to (32/9)\alpha^2/\alpha_s^2 \sim (1-2)\times 10^{-2}$, depending upon the m_{P^0}-dependent value of α_s employed. In particular,

$$\Gamma(P^0 \to gg)B(P^0 \to \gamma\gamma) \to \frac{2\alpha^2}{27\pi^3}\frac{N_{TC}^2 m_{P^0}^3}{v^2} \sim 2.4 \times 10^{-3}\ \mathrm{MeV} N_{TC}^2 \left(\frac{m_{P^0}}{100\ \mathrm{GeV}}\right)^3 , \tag{36}$$

which is typically much larger than the corresponding result for a SM-like Higgs boson. This makes P^0 discovery in the $\gamma\gamma$ final state at a hadron collider much easier than in the SM Higgs case. Similarly, one finds a larger value of $\Gamma(P^0 \to \gamma\gamma)B(P^0 \to b\overline{b})$ as compared to the SM h analogue. This implies that discovery of the P^0 in $\gamma\gamma$ collisions will be much easier than for a SM Higgs boson. The large values of the P^0/h ratios for these two ΓB combinations are illustrated in Fig. 3.

We note that these ratios are quite sensitive to the composition of the P^0 mass-eigenstate. In particular, if the π_D isosinglet state were the mass-eigenstate, the phenomenologically relevant products $\Gamma(\pi_D \to gg)B(\pi_D \to \gamma\gamma)$ and $\Gamma(\pi_D \to \gamma\gamma)B(\pi_D \to b\overline{b})$ would be smaller by factors of about 8 and 8/3, respectively, compared to their P^0 counterparts. Thus, both products would still be larger than their respective SM Higgs analogues, but not so dramatically as for the P^0 eigenstate.

It is the large P^0/h ratios for the ΓB combinations discussed above in combination with the fact that the P^0 can naturally have a low mass that makes the P^0 such a unique object. With this summary of the couplings and basic properties of the P^0, we are now in a position to consider its phenomenology at various colliders.

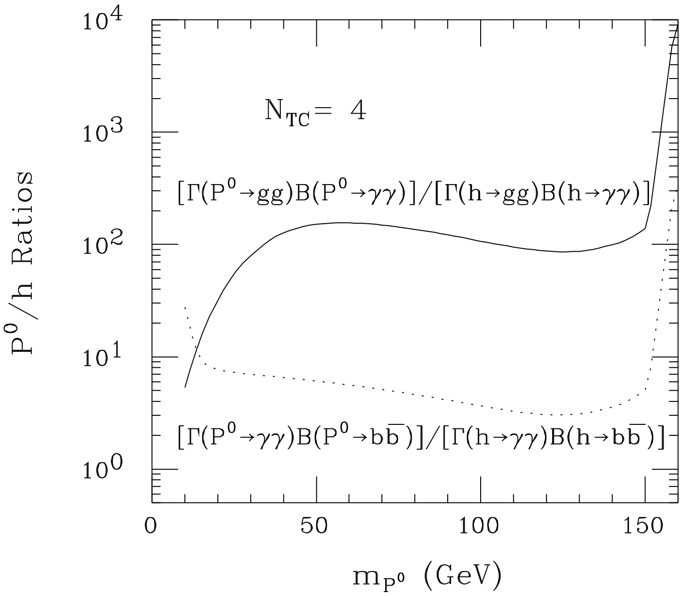

Figure 3: The ratios $[\Gamma(P^0 \to gg)B(P^0 \to \gamma\gamma)]/[\Gamma(h \to gg)B(h \to \gamma\gamma)]$ and $[\Gamma(P^0 \to \gamma\gamma)B(P^0 \to b\bar{b})]/[\Gamma(h \to \gamma\gamma)B(h \to b\bar{b})]$, where h is the SM Higgs boson, are plotted as a function of m_{P^0}, taking $m_h = m_{P^0}$. Results assume $N_{TC} = 4$ and the specific P^0 couplings of Eqs. (27), (29) and (32).

4 P^0 production at the Tevatron and the LHC

In this section, we discuss the ability of the Tevatron and LHC to discover the PNGB's. We focus primarily on the P^0 since, as we have seen, it is the lightest of the PNGB's and, therefore, possibly the only PNGB that can be produced and studied at first-generation e^+e^- and $\mu^+\mu^-$ colliders.

The most important discovery mode for the P^0 at the Tevatron and the LHC is almost certainly production via inclusive $gg \to P^0$ fusion followed by $P^0 \to \gamma\gamma$ decay. This is the same production/decay mode as considered for a light Standard Model Higgs boson, h. Indeed, although this mode has been hitherto received little attention, it is even more robust for the P^0 than for the SM h, and is possibly viable at the Tevatron as well as at the LHC. This is because the rate for the $gg \to R \to \gamma\gamma$ channel ($R = P^0$ or h) is proportional to $\Gamma(R \to gg)B(R \to \gamma\gamma)$ and, as illustrated in Fig. 3 in the previous section, both factors are larger for the P^0 than for the h. Even for the modest value of $N_{TC} = 4$ we employ, the P^0/h ratio is greater than 10 for $m_{P^0} \gtrsim 12$ GeV rising to > 100 once $m_{P^0} > 30$. For large $m_{P^0} \gtrsim 150$ GeV, the ratio becomes very large as a result of the precipitous decline of $B(h \to \gamma\gamma)$ for the SM h due to the opening up of the $h \to WW, ZZ$ decay modes, which are absent or negligible (respectively) in the case of the P^0. In fact, Fig. 1 and Eq. (36) make it clear that $\Gamma(P^0 \to gg)B(P^0 \to \gamma\gamma)$ is roughly constant for large $m_{P^0} \geq 150$ GeV, implying a signal rate that decreases at large m_{P^0} only as a result of phase space and decreasing gluon distribution functions.

Let us first consider the LHC. We recall that the LHC ATLAS [29] and CMS [30] studies claim that the SM Higgs boson can be discovered using the $gg \to h \to \gamma\gamma$ mode in the $m_h > 70$ GeV mass region, extending up to about 150 GeV, where the upper limit derives entirely from the steep decline in $B(h \to \gamma\gamma)$ that occurs when the $h \to WW, ZZ$ decay modes open up. Thus, from Fig. 3 we feel it is safe to conclude that, for $N_{TC} \geq 4$, the P^0 can be detected in the $gg \to P^0 \to \gamma\gamma$ mode for at least $50 < m_{P^0} < 200$ GeV. The background studies by the detector collaborations required to determine if the discovery region is even larger are not available. We expect that discovery will be possible for a substantial range above 200 GeV because of the rapid decline in the background rate as $M_{\gamma\gamma}$ increases. Extension of the discovery range to lower $m_{P^0} < 50$ GeV will be limited by the rapid rise in the irreducible $\gamma\gamma$ background at small $M_{\gamma\gamma}$ and the increased difficulty in rejecting the reducible γ-jet and jet-jet backgrounds that arise when the jets fluctuate so as to look like a photon. A detailed study by the ATLAS and CMS collaborations is in order.

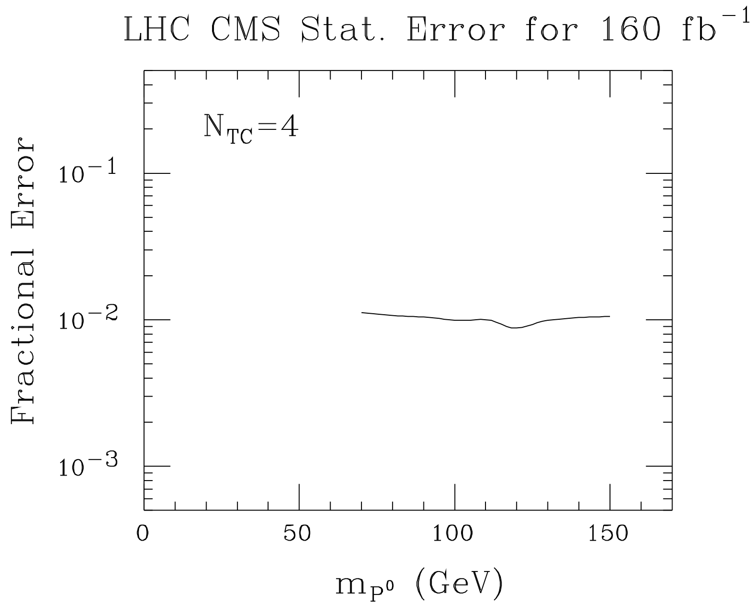

Figure 4: The fractional statistical error $(S+B)^{1/2}/S$ for the $gg \to P^0 \to \gamma\gamma$ rate, assuming $N_{TC} = 4$ and $L = 160$ fb^{-1} of accumulated luminosity at the LHC. Results are based on the rates quoted by CMS for the SM Higgs boson when only events containing at least two high E_T (central) or high E (forward) jets are accepted. The $gg \to P^0 \to \gamma\gamma$ signal rate S is computed from the SM Higgs rate by multiplying by the appropriate factor at each m_{P^0} as plotted in Fig. 3.

As we shall see in later sections, the $gg \to P^0 \to \gamma\gamma$ LHC mode will be an important ingredient in determining the parameters of the technicolor model. Thus, we wish to estimate the statistical errors for the measurement of the associated rate. We consider P^0 masses for which the appropriate LHC background and $M_{\gamma\gamma}$ resolution results are available. Since the CMS $M_{\gamma\gamma}$ resolution is typically better than that which will be achieved by ATLAS, we will employ the results of the CMS technical proposal [30] from their Table 12.2, which covers the mass range $70-150$ GeV and assumes an integrated luminosity of $L = 160$ fb^{-1}. The signal and background rates quoted in Table 12.2 are those for the preferred method in which one accepts only $\gamma\gamma$ events that contain at least two jets with either high E_T (for central jets) or high E (for forward jets). Detailed requirements may be found in Ref. [30]. At each mass, we use the S value for the SM Higgs boson from the CMS Table 12.2 and the results of Fig. 3 to compute the expected S for the P^0. We then use this modified S and the B value from the CMS Table 12.2 to compute $(S+B)^{1/2}/S$. The resulting fractional statistical error is plotted as a function of m_{P^0} in Fig. 4. After the adjustment described to scale the SM Higgs rate up to the expected P^0 signal rate, we find a statistical error for measurement of the $gg \to P^0 \to \gamma\gamma$ rate that is essentially constant at $\sim 1\%$. It seems likely that this $\sim 1\%$ error will apply beyond the mass range for which specific CMS SM Higgs boson studies have been performed, with deterioration expected at small m_{P^0}. Overall, we can anticipate that the $gg \to P^0 \to \gamma\gamma$ rate will be measured with substantial statistical accuracy for almost the entire mass range for which discovery is possible. Indeed, systematic uncertainty associated with normalizing the absolute rate (after cuts) will almost certainly dominate for all but small m_{P^0}.

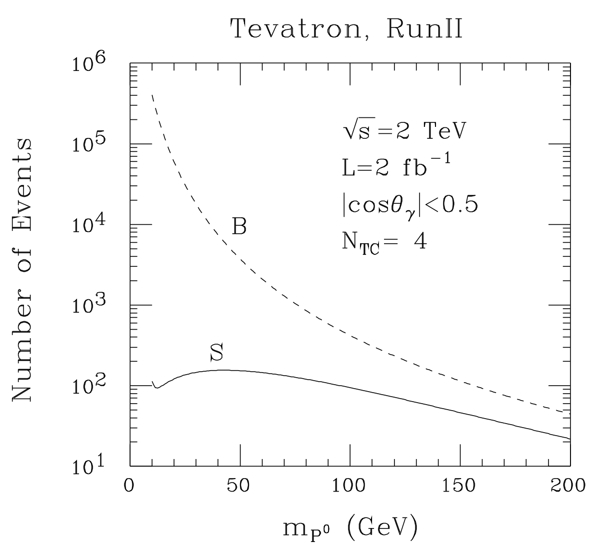

Figure 5: The $gg \to P^0 \to \gamma\gamma$ signal rate S is plotted as a function of m_{P^0} for $N_{TC} = 4$ in the case of $\sqrt{s} = 2$ TeV and $L = 2$ fb^{-1} at the Tevatron. Also shown is the irreducible background rate, B, obtained by multiplying $d\sigma(p\overline{p} \to q\overline{q} \to \gamma\gamma)/dM_{\gamma\gamma}$ by a factor of 1.5 to include the $gg \to \gamma\gamma$ loop contribution and by a mass interval size of $2\Delta M_{\gamma\gamma}$, where $\Delta M_{\gamma\gamma}$ is computed for $\Delta E_\gamma/E_\gamma = 0.135/\sqrt{E_\gamma} \oplus 0.015$. In computing both S and B, we required the final state photons to have $|\cos\theta_\gamma| < 0.5$.

Given the substantial enhancement of the $gg \to P^0 \to \gamma\gamma$ rate relative to the case of the SM h, it is also possible that this mode is viable at the Tevatron, even though for the SM h it is not. In order to assess the prospects, we have computed signal and irreducible background rates for RunII parameters, requiring that both of the final-state photons have $|\cos\theta_\gamma| < 0.5$. The P^0 event rate for $N_{TC} = 4$ is plotted in Fig. 5; the rate is sizeable for the assumed $L = 2~\mathrm{fb}^{-1}$. The background rate shown is that computed using $B = 1.5[d\sigma(p\overline{p} \to q\overline{q} \to \gamma\gamma)/dM_{\gamma\gamma}][2\Delta M_{\gamma\gamma}]$, where we use a $\gamma\gamma$ invariant mass window of $2\Delta M_{\gamma\gamma}$ with $\Delta M_{\gamma\gamma}/M_{\gamma\gamma} = \frac{1}{\sqrt{2}}\Delta E_\gamma/E_\gamma$. Here, we employ $\Delta E_\gamma/E_\gamma = 0.135/\sqrt{E_\gamma} \oplus 0.015$ [32] with $E_\gamma = m_{P^0}/2$. The factor of 1.5 in B above is included in order to approximately account for the well-known [31] $p\overline{p} \to gg \to \gamma\gamma$ one-loop contribution to the inclusive $\gamma\gamma$ background.

In addition to the irreducible $\gamma\gamma$ background, there may be reducible backgrounds deriving from γj and jj final states in which the j fragments in such a way that it is identified as a γ (*e.g.* $j \to$ fast π^0) [33]. These must be eliminated/reduced by using very tight cuts and requirements to define a (prompt) isolated photon. Roughly, it is necessary that the cuts discriminate at a level of one part in 10^4 against a jet which fluctuates in such a way as to look like a photon as opposed to a directly produced photon. ALEPH and RunI Tevatron results [34] suggest that the per-jet discrimination factor of $\sim 10^{-4}$ can be achieved for relatively energetic photons. However, at low m_{P^0} the photon energies are not large and the jet-γ discrimination factor worsens. A detailed detector simulation is required in order to assess the magnitude of such reducible backgrounds as a function of m_{P^0}. Here, we note only that both S and the irreducible background B will be reduced compared to Fig. 5 by the efficiency of the cuts/requirements imposed in order to eliminate these reducible $j \to \gamma$ fluctuation backgrounds.

As a very first indication of whether P^0 discovery during RunII at the Tevatron is possible in the $\gamma\gamma$ mode, we present in Fig. 6 results for $N_{SD} = S/\sqrt{B}$, computed using the signal and background rates S and B plotted in Fig. 5, which were obtained assuming $N_{TC} = 4$ and $L = 2~\mathrm{fb}^{-1}$. We see that $N_{SD} \gtrsim 3$ is achieved for $m_{P^0} \gtrsim$ 60 GeV. For $m_{P^0} \sim 60, 100, 150, 200$ GeV, the statistical fractional error for $\Gamma(P^0 \to gg)B(P^0 \to \gamma\gamma)$ (computed as $\sqrt{S+B}/S$) is $0.33, 0.24, 0.27, 0.37$, respectively.

For TeV33 luminosity of $L = 30~\mathrm{fb}^{-1}$, it may prove possible to probe lower m_{P^0}, pending the outcome of detailed studies of mass resolution and jet-γ discrimination at lower $M_{\gamma\gamma}$. At TeV33, discovery of the P^0 would certainly be possible for $m_{P^0} \gtrsim$ 60 GeV, and the factor of 15 increase in luminosity would allow reasonable precision ($\pm 5\% - \pm 10\%$) for the determination of $\Gamma(P^0 \to gg)B(P^0 \to \gamma\gamma)$.

Of course, it is very interesting to know if RunI results could place any constraints on the P^0. To assess this, we present in Fig. 7 a plot of $\sigma(p\overline{p} \to gg \to P^0)B(P^0 \to \gamma\gamma)$ (taking $N_{TC} = 4$) at $\sqrt{s} = 1.8$ TeV; no efficiency reductions or cuts are included. We see that with $L = 100~\mathrm{pb}^{-1}$ the raw number of events will range from ~ 10 at $m_{P^0} \sim 40$ GeV down to ~ 2 at $m_{P^0} \sim 200$ GeV. These numbers will be further reduced by efficiency factors associated with requiring central rapid-

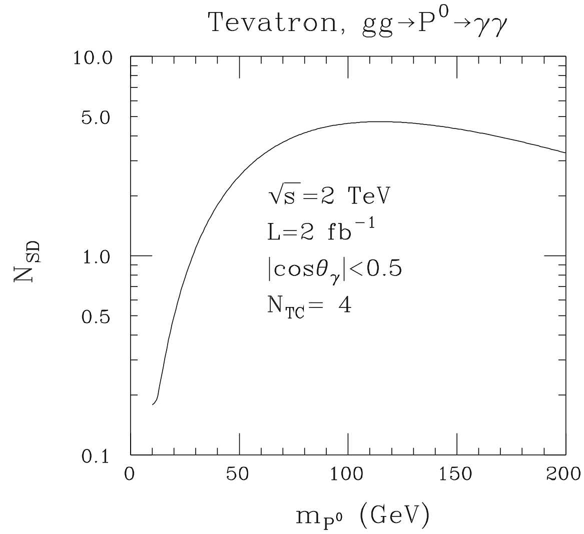

Figure 6: The $gg \to P^0 \to \gamma\gamma$ signal significance, $N_{SD} = S/\sqrt{B}$, is plotted as a function of m_{P^0} for $\sqrt{s} = 2$ TeV and $L = 2$ fb^{-1} at the Tevatron using S and B as plotted in Fig. 5.

ity for the photons and removing the reducible backgrounds from γj and jj events. Consequently, we anticipate that obtaining useful constraints on the P^0 from RunI data will be very difficult for moderate N_{TC} values.

We can roughly verify the above expectation by using analyzes of the inclusive $\gamma\gamma$ mass spectrum from RunI that have already appeared. For example, Ref. [35] gives (Fig. 1) results for $dN(p\overline{p} \to \gamma\gamma)/dM_{\gamma\gamma}$ for $40 \leq M_{\gamma\gamma} \leq 350$ GeV and (Fig. 3) resulting limits on $d\sigma(p\overline{p} \to \gamma\gamma)/dM_{\gamma\gamma}$ (where the experimental results have been corrected for cuts and efficiencies to obtain the raw cross section) in the mass range from $100 - 350$ GeV. We consider first the Fig. 3 limits. After integrating over the mass bins shown in Fig. 3 of Ref. [35], which range in size from 15 GeV for $M_{\gamma\gamma} \sim 120$ GeV to 30 GeV at $M_{\gamma\gamma} \sim 200$ GeV, one obtains $\sigma(p\overline{p} \to \gamma\gamma)$ limits of order 0.7 pb and 0.3 pb for these respective mass bins. From Fig. 7, we see that sensitivity would have to be increased by about a factor of 10 in order to place limits on the P^0 for $N_{TC} = 4$ using this approach. Possibly of greater utility is the smaller binning of their Fig. 1. We consider the situation for a few representative values of $M_{\gamma\gamma}$.

- At $M_{\gamma\gamma} = 100$ GeV, $dN(p\overline{p} \to \gamma\gamma)/dM_{\gamma\gamma} \sim (0.25 + 0.15 - 0.25)$/GeV. Multiplying the upper limit by the bin size, ~ 4 GeV, gives $N \leq 1.6$ events in this bin (at the 1σ level). The expected QCD background (including fakes) in this bin is, from Fig. 2 of [35], $N \sim 2.4$. The expected ($N_{TC} = 4$) P^0 signal in this bin is $N = \epsilon L\sigma \sim 0.8$, using $\epsilon \sim 0.105$ [35], $L \sim 100$ pb^{-1} and $\sigma(p\overline{p} \to P^0 \to \gamma\gamma) \sim 0.074$ pb (Fig. 7).

- At $M_{\gamma\gamma} = 200$ GeV, $dN(p\overline{p} \to \gamma\gamma)/dM_{\gamma\gamma} \lesssim 0.01$/GeV. Multiplying by the

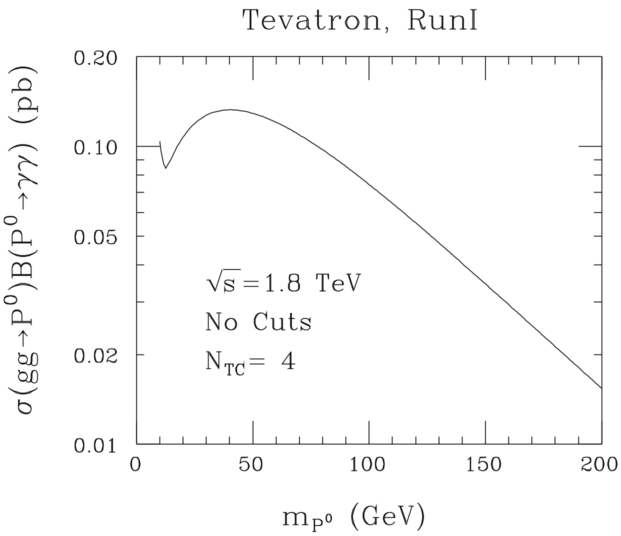

Figure 7: $\sigma(p\overline{p} \to gg \to P^0)B(P^0 \to \gamma\gamma)$ is plotted as a function of m_{P^0} for $\sqrt{s} = 1.8$ TeV at the Tevatron. $N_{TC} = 4$ is assumed. No cuts are placed on the γ's.

bin size, ~ 8 GeV, gives $N \leq 0.08$ events in this bin. The expected QCD background in this bin is $N \sim 0.24$. The expected P^0 signal in this bin is $N \sim 0.2$, as obtained using $\epsilon \sim 0.125$ [35] and $\sigma(p\overline{p} \to P^0 \to \gamma\gamma) \sim 0.015$ pb.

- At $M_{\gamma\gamma} = 50$ GeV, a bin size of ~ 2.5 GeV gives $N \sim 25$ events, with an expected background of $N \sim 25$. Extrapolating linearly the efficiencies given in Ref. [35] for $100-300$ GeV down to 50 GeV gives $\epsilon \sim 0.095$ and an expected signal rate of $N \sim 1.2$.

These estimates make it clear that, for $N_{TC} = 4$, a P^0 is still allowed for any mass below 200 GeV. However, it is also apparent that the factor 20 increase in luminosity expected for RunII will allow either exclusion or discovery of an $N_{TC} = 4$ P^0 in the $100 - 200$ GeV mass range, with extension to masses as low as 50 GeV requiring improved procedures for removing fakes.

Of course, since the signal rate scales as N_{TC}^2 [see Eq. (36)] (or faster at m_{P^0} values low enough that $B(P^0 \to \gamma\gamma)$ has not yet saturated), the RunI limits do allow us to exclude the presence of a P^0 if N_{TC} is large. For example, if $N_{TC} = 12$, the number of signal events is at least 9 times larger than quoted above for $N_{TC} = 4$. For the most favorable mass, $m_{P^0} = 100$ GeV, $N_{TC} = 12$ would yield ~ 7 events where ≤ 1.6 are seen and ≤ 2.4 are expected from background. $N_{TC} = 16$ or so would be required in order that a P^0 with $m_{P^0} = 50$ or 200 GeV have low probability. A detailed determination of m_{P^0} mass ranges that can be excluded (using RunI data) as a function of N_{TC} should be performed by the CDF and D0 detector groups.

Our overall conclusion is that there is significant potential for discovering and studying the P^0 at the Tevatron using the $gg \to P^0 \to \gamma\gamma$ production/decay mode. Our cursory analysis suggests that RunI data can be used to exclude a P^0 in the

$50 - 200$ GeV mass range for $N_{TC} \geq 12 - 16$ (depending upon mass). Given that production rates and branching ratios depend significantly on N_{TC}, a detailed analysis by the detector groups of the maximum N_{TC} allowed by the RunI data as a function of m_{P^0} would provide very important guidance for future searches. Note that were the isosinglet π_D the mass eigenstate, the $gg \to \pi_D \to \gamma\gamma$ rate would be much less enhanced and prospects at the Tevatron would be much worse.

The second decay mode that can be considered for discovering the P^0 in inclusive gluon-fusion production is $\tau^+\tau^-$. However, the early claims [3] that the $\tau^+\tau^-$ decay mode would easily allow discovery have not been substantiated; backgrounds and inefficiencies associated with τ pair reconstruction are the main difficulties.

One can also consider searching for the P^0 in the γP^0 and ZP^0 channels. (Since the WW coupling to the P^0 is zero, the WP^0 channel is not present.) For moderate N_{TC}, the much smaller ZZ coupling of the P^0 as compared to a SM-like Higgs implies that the ZP^0 cross section will be greatly reduced relative to the Higgs case. Consequently, the RunI limits for the $Z\gamma\gamma$ mode given in Ref. [35] will only constrain the P^0 when N_{TC} is quite large. An analysis as a function of N_{TC} is in order. The cleanliness of the $\gamma\gamma\gamma$ channel (see Ref. [36], for example) suggests that it too deserves a detailed examination. For low m_{P^0}, the $\gamma\tau^+\tau^-$ and $Z\tau^+\tau^-$ channels might prove useful at large N_{TC}. We defer an examination of all these channels to a later work.

Most studies of PNGB detection at hadron colliders have focused on the production of pairs of PNGB's. Aside from simple Drell-Yan pair production via γ and Z exchange, there is the possibility of resonant production $pp \to V^\pm X \to P^\pm P^0 X$ or $pp \to V^0 X \to P^\pm P^\mp X$ [4], where V is a vector resonance such as the technirho (see the introduction). For the type of model we consider here, the technirho has mass in the TeV range. Further, it will not be particularly narrow and it will have many competing decay modes. In addition, one will need to find the two PNGB's in channels such as $P^+ \to c\overline{b}$ and $P^0 \to b\overline{b}$ or gg that have large backgrounds and poor mass resolution. To date, there is no study showing that PNGB pairs can be detected when the technirho is heavy. More detailed studies will be needed to fully clarify the prospects. Thus, Ref. [7] concluded that the Drell-Yan production of pairs of color-singlet PNGB's is unobservably small compared to backgrounds *unless* there is one or more fairly strong color-singlet technirho and/or techniomega resonances not far above threshold. If the technirho is not far above threshold, then, for example, $\rho_T^\pm \to W^\pm P^0$ can be the dominant decay. The $\rho_T^\pm$ is then sufficiently narrow that cuts on the data can be made which bring out the signal, as found in Ref. [8]. Similarly, for a light techniomega, $pp \to \omega_T X \to \gamma P^0 X$ can be the dominant channel and [8] finds that a viable signal is possible after suitable cuts.

One could also consider the process $pp \to gg \to P^0 P^0$, mediated by the anomalous ggP^0 vertex. The main kinematic trick would be to look for equal mass pairs. However, backgrounds in the four jet channel will be very large.

Thus, unless the technirho (or techniomega) is much lighter than expected in the model we consider here, the best mode for P^0 discovery at the Tevatron and

LHC is $gg \to P^0 \to \gamma\gamma$. This mode is clearly viable for $m_{P^0} \gtrsim 50$ GeV (up to masses somewhat above 200 GeV). Viability will probably extend to substantially lower m_{P^0} at the LHC and possibly to somewhat lower m_{P^0} for TeV33 luminosity at the Tevatron — detailed detector simulations of backgrounds and $M_{\gamma\gamma}$ resolution at low m_{P^0} will be required to confirm these expectations. It is in this context that we consider the role of electron and muon colliders for the discovery and eventual study of the P^0.

5 P^0 production at an electron collider

In this section, we give a brief overview of the role that an e^+e^- collider might play in the study and discovery of the P^0. As we have already noted, the partner $P^{0\prime}$ state with one-loop mass proportional to the t-quark mass will, most naturally, be much heavier and, thus, would have much smaller cross section. For an ultra-violet cut-off scale, Λ, of order 2 TeV or larger (the most natural range for a technicolor model), the $P^{0\prime}$ would be too heavy to be produced even at a $\sqrt{s} \lesssim 500$ GeV collider. Although we shall employ the specific P^0 properties, in particular branching fractions and couplings, as predicted by the scheme reviewed earlier, strategies for probing the lightest PNGB in other models of a strongly interacting electroweak sector would generally not be all that different. In e^+e^- collisions, the greatest differences would arise from two sources. First, if the eigenstate composition of the lightest PNGB were not that of the P^0, then, as noted earlier, the (very crucial) $\gamma\gamma$ coupling-squared could be very different, *e.g.* a factor of 8 smaller if the lightest PNGB were the π_D. This would reduce the two most relevant cross sections by a factor of 8. Second, in models such as walking technicolor results would be altered due to: (a) the possibility that m_{P^0} is substantially larger for the same Λ; and (b) the larger $P^0\gamma\gamma$ and $P^0 Z\gamma$ couplings as a result of a smaller effective scale in place of v in Eq. (28).

First, let us consider whether LEP places any limits on the P^0. At LEP the dominant production mode is $Z \to \gamma P^0$. The width for this decay is given by

$$\Gamma(Z \to \gamma P^0) = \frac{\alpha^2 m_Z^3}{96\pi^3 v^2} N_{TC}^2 A_{P^0 Z\gamma}^2 \left(1 - \frac{m_{P^0}^2}{m_Z^2}\right)^3 , \tag{37}$$

where $A_{P^0 Z\gamma}$ appeared in Eq. (30). Let us follow Ref. [5] and require that the $Z \to \gamma P^0$ decay width be $> 2 \times 10^{-6}$ GeV in order for the P^0 to be visible in a sample of 10^7 Z bosons. The minimum N_{TC} value required as a function of m_{P^0} is plotted in Fig. 8. We see that $N_{TC} \gtrsim 8$ is required at $m_{P^0} = 0$, rising rapidly as m_{P^0} increases.[6]

We next consider LEP2. The general form of the cross section for PV production

[6]In a multi-scale model, where the effective v could be smaller, these results would be altered.

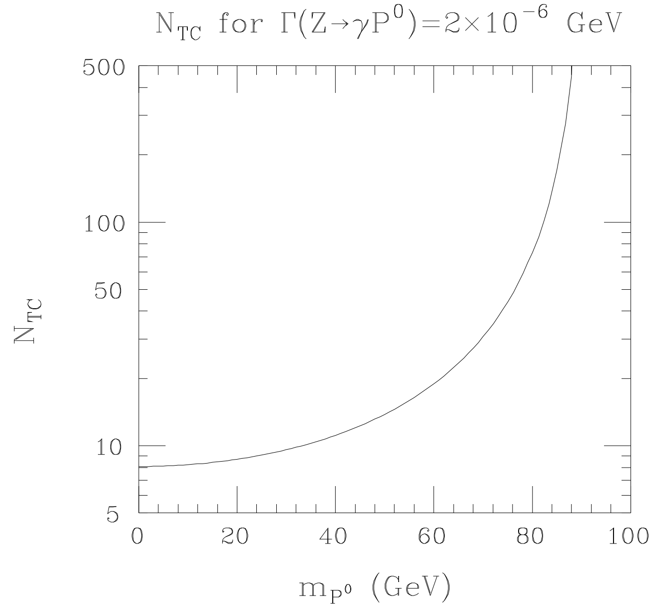

Figure 8: The value of N_{TC} required for $\Gamma(Z \to \gamma P^0) > 2 \times 10^{-6}$ GeV is plotted as a function of m_{P^0}.

(from Ref. [9]) is

$$\begin{aligned}\sigma(e^+e^- \to PV) &= \frac{\alpha^3 N_{TC}^2}{24\pi^2 v^2}\lambda^{3/2}(1, m_P^2/s, m_V^2/s) \\ &\times \left[A_{PV\gamma}^2 + \frac{A_{PV\gamma}A_{PVZ}(1-4s_W^2)}{2c_w s_W(1-m_Z^2/s)} + \frac{A_{PVZ}^2(1-4s_w^2+8s_W^4)}{8c_W^2 s_W^2(1-m_Z^2/s)^2}\right], \end{aligned} \qquad (38)$$

where $V = \gamma, Z$ and P is the PNGB. In the above, we have neglected the Z width. As already stated, the best mode for P^0 production at an e^+e^- collider (with $\sqrt{s} > m_Z$) is $e^+e^- \to \gamma P^0$. Because the $P^0 Z\gamma$ coupling-squared is much smaller than the $P^0\gamma\gamma$ coupling-squared (by a factor of nearly 400), the dominant diagram is $e^+e^- \to \gamma \to \gamma P^0$, proportional to $A^2_{P^0\gamma\gamma}$. Even when kinematically allowed, rates in the $e^+e^- \to ZP^0$ channel are substantially smaller, as we shall discuss. We will give results for the moderate value of $N_{TC} = 4$. For $\sqrt{s} = 200$ GeV, we find that, after imposing an angular cut of $20^\circ \le \theta \le 160^\circ$ on the outgoing photon (a convenient acceptance cut that also avoids the forward/backward cross section singularities but is more than 91% efficient), the $e^+e^- \to \gamma P^0$ cross section is below 1 fb for $N_{TC} = 4$. Given that the maximum integrated luminosity anticipated is of order $L \sim 0.5$ fb^{-1}, we conclude that LEP2 will not allow detection of the P^0 unless N_{TC} is very large.

The cross section for $e^+e^- \to \gamma P^0$ at $\sqrt{s} = 500$ GeV, after imposing the same angular cut as for LEP2, is illustrated in Fig. 9. It ranges from 0.9 fb down to 0.5 fb as m_{P^0} goes from zero up to ~ 200 GeV. For $L = 50$ fb^{-1}, we have at most 45 events with which to discover and study the P^0. The $e^+e^- \to ZP^0$ cross section is even

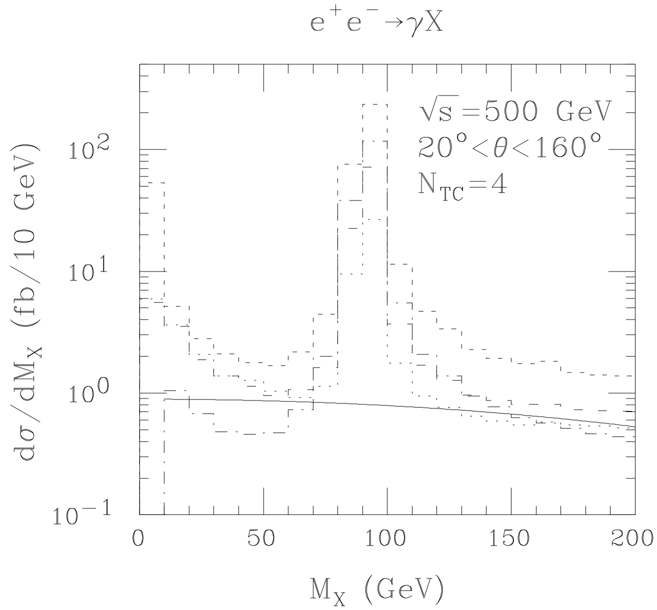

Figure 9: The cross section (in fb) for $e^+e^- \to \gamma P^0$ (solid curve) is plotted as a function of m_{P^0} in comparison to various possible backgrounds: $e^+e^- \to \gamma b\overline{b}$ (dotdash); $e^+e^- \to \gamma c\overline{c}$ (dashes); $e^+e^- \to \gamma q\overline{q}$, $q = u, d, s$ (small dashes); and $e^+e^- \to \gamma\tau^+\tau^-$ (dots). The background cross sections are integrated over a $\Delta M_X =$ 10 GeV bin width (a possible approximation to the resolution that can be achieved). A cut of $20° \leq \theta \leq 160°$ has been applied to both the signal and the backgrounds. Effects due to tagging and mis-tagging are discussed in the text.

smaller. Without cuts and without considering any specific Z or P^0 decay modes, it ranges from 0.014 fb down to 0.008 fb over the same mass range. With less than 1 event to work with, there is little point in examining the ZP^0 mode. If TESLA is able to achieve $L = 500$ fb^{-1} per year, γP^0 production will have a substantial rate, but the ZP^0 production rate will still not be useful.

In order to assess the γP^0 situation more fully, we must consider backgrounds. As we have seen, the dominant decay of the P^0 is typically to $b\overline{b}$, $\tau^+\tau^-$ or gg. For the $b\overline{b}$ and gg modes, the backgrounds relevant to the γP^0 channel are $\gamma b\overline{b}$, $\gamma c\overline{c}$ and $\gamma q\overline{q}$ ($q = u, d, s$) production. The cross sections for these processes obtained after integrating over a 10 GeV bin size in the quark-antiquark mass (an optimistic estimate of the resolution that could be achieved using reconstruction of the quark-antiquark or $\tau^+\tau^-$ pair) are also given in Fig. 9. For $10 \lesssim m_{P^0} \lesssim 80$ GeV and $m_{P^0} \geq 100$ GeV, the signal to background ratio is not too much smaller than 1. We will assess the P^0 discovery potential in specific channels by assuming that 10 GeV mass resolution can be achieved for m_{P^0} in each case.

In order to proceed with a discussion of specific final states, we must state our assumptions regarding tagging and mis-tagging efficiencies. We separate $\tau^+\tau^-$, $b\overline{b}$, $c\overline{c}$ and $q\overline{q}/gg$ final states by using topological and τ tagging with efficiencies and mis-tagging probabilities as estimated by B. King [37] for the muon collider. These are a bit on the pessimistic side for an e^+e^- collider, but only slightly so. We take $\epsilon_{bb} = 0.55$, $\epsilon_{cc} = 0.38$, $\epsilon_{bc} = 0.18$, $\epsilon_{cb} = 0.03$, $\epsilon_{qb} = \epsilon_{gb} = 0.03$, $\epsilon_{qc} = \epsilon_{gc} = 0.32$, $\epsilon_{\tau\tau} = 0.8$, $\epsilon_{\tau b} = \epsilon_{\tau c} = \epsilon_{\tau q} = 0$, where the notation is that ϵ_{ab} is the probability that a particle/jet of type a is tagged as being of type b. Gluons are treated the same as light quarks. Note that $\epsilon_{bq} = 1 - \epsilon_{bb} - \epsilon_{bc}$, $\epsilon_{cq} = 1 - \epsilon_{cc} - \epsilon_{cb}$, and $\epsilon_{qq} = 1 - \epsilon_{qb} - \epsilon_{qc}$.

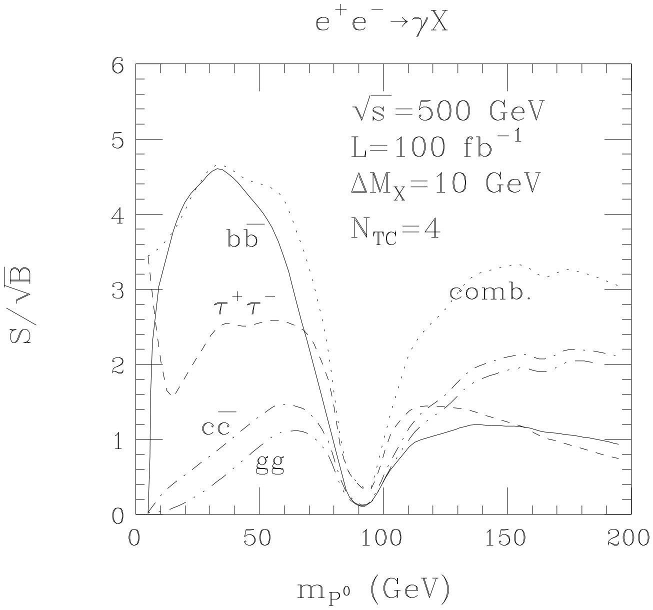

Figure 10: We consider $e^+e^- \to \gamma X$ and, for $L = 100$ fb^{-1} at $\sqrt{s} = 500$ GeV, plot the statistical significances $S/\sqrt{B}$ for a P^0 signal in various 'tagged' channels as a function of m_{P^0}. We assume mass resolution of $\Delta M_X = 10$ GeV in each channel and the channel tagging and mis-tagging probabilities discussed in the text. A cut of $20° \leq \theta \leq 160°$ has been imposed on both the signal and the backgrounds. The curve legend is: gg (dot-dot-dash); $c\overline{c}$ (dot-dash); $b\overline{b}$ (solid); $\tau^+\tau^-$ (dashes). Also shown (dots) is the largest $S/\sqrt{B}$ that can be achieved by considering all possible combinations of channels.

We then identify final states according to the following scheme. A final state is identified as: $b\overline{b}$ if one or more jets is tagged as a b; $c\overline{c}$ if no jet is tagged as a b, but one or more jets is tagged as a c; and $q\overline{q}/gg$ if neither jet is tagged as a b or a c. Background and signal events are analyzed in exactly the same manner. Note, in particular, that even though the P^0 does not decay to $c\overline{c}$, some of its $b\overline{b}$ and gg decays will be identified as $c\overline{c}$. These individual jet tagging and mis-tagging efficiencies then lead to the following final state efficiencies: $\epsilon_{bb/bb} = 0.8$, $\epsilon_{bb/cc} = 0.13$, $\epsilon_{bb/qq} \sim 0$, $\epsilon_{cc/cc} = 0.6$, $\epsilon_{cc/bb} = 0.04$, $\epsilon_{cc/qq} = 0.36$, $\epsilon_{qq/qq} = 0.42$, $\epsilon_{qq/bb} = 0.06$, $\epsilon_{qq/cc} = 0.52$, $\epsilon_{\tau\tau/\tau\tau} = 0.96$. Here, the notation is that $\epsilon_{aa/bb}$ is the probability that a final state that is truly aa is tagged as the final state bb. We give some examples of how the above channel efficiencies are computed. For instance,

$\epsilon_{bb/bb} = 1 - (1 - \epsilon_{bb})^2$, $\epsilon_{bb/cc} = 2\epsilon_{bc}\epsilon_{bq} + \epsilon_{bc}^2$, $\epsilon_{bb/qq} = (1 - \epsilon_{bb} - \epsilon_{bc})^2$, with the sum of these three tagging probabilities being 1. The $c\overline{c}$ final state is treated similarly. For the qq (or gg) final state we have $\epsilon_{qq/qq} = (1 - \epsilon_{qb} - \epsilon_{qc})^2$, $\epsilon_{qq/bb} = 2\epsilon_{qb}(1 - \epsilon_{qb}) + \epsilon_{qb}^2$, and $\epsilon_{qq/cc} = 2\epsilon_{qc}(1 - \epsilon_{qc} - \epsilon_{qb}) + \epsilon_{qc}^2$; again one can check that these sum to 1.

Results for $S/\sqrt{B}$, in the various tagged channels, assuming $L = 100\ \mathrm{fb}^{-1}$ at $\sqrt{s} = 500$ GeV, are plotted in Fig. 10. We have assumed a mass window of $\Delta M_X = 10$ GeV in evaluating the backgrounds in the various channels. Also shown in Fig. 10 is the largest $S/\sqrt{B}$ that can be achieved by considering (at each m_{P^0}) all possible combinations of the gg, $c\overline{c}$, $b\overline{b}$ and $\tau^+\tau^-$ channels. From the figure, we find $S/\sqrt{B} \geq 3$ (our discovery criterion) for $m_{P^0} \leq 75$ GeV and $m_{P^0} \geq 130$ GeV, *i.e.* outside the Z region. A strong signal, $S/\sqrt{B} \sim 5$, is only possible for $m_{P^0} \sim 40$ GeV. As the figure shows, the signal in any one channel is often too weak for discovery, and it is only the best channel combination that will reveal a signal. For the TESLA $L = 500\ \mathrm{fb}^{-1}$ luminosity, $S/\sqrt{B}$ should be multiplied by ~ 2.2 and discovery prospects will be improved.

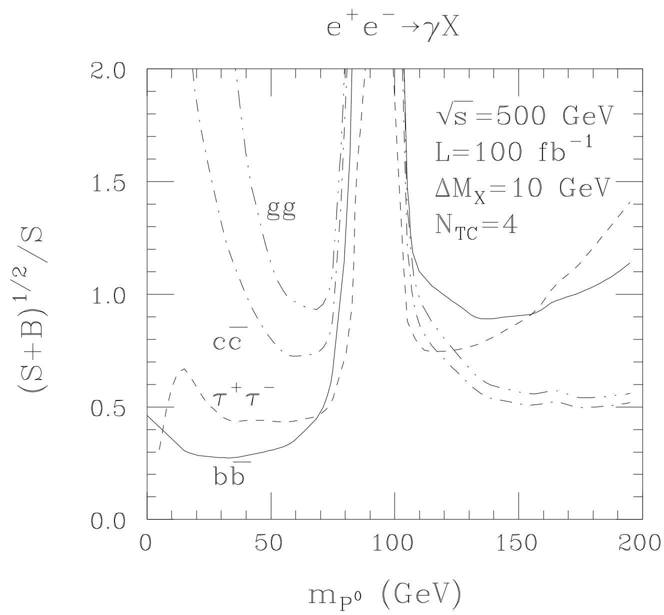

Figure 11: We consider $e^+e^- \to \gamma P^0 \to \gamma X$ production, with $L = 100\ \mathrm{fb}^{-1}$ at $\sqrt{s} = 500$ GeV, and plot the statistical error $(S + B)^{1/2}/S$ for the various 'tagged' channel rates ($X = \tau^+\tau^-$, $b\overline{b}$, $c\overline{c}$, gg) as a function of m_{P^0}. Assumptions and notation as in Fig. 10.

Once a PNGB is discovered, one will wish to determine the branching fractions and couplings as precisely as possible in order to pin down the fundamental parameters of the model. In the $e^+e^- \to \gamma P^0$ production mode, one will begin by extracting ratios of branching fractions by computing ratios of the rates measured in various final state channels.[7] As a first indication of how well one can do, we give, in Fig. 11, the statistical errors $(S+B)^{1/2}/S$ in each of the tagged channels in the case of our bench mark example of the P^0. Even if we decrease the errors of the figure by the $\sqrt{5} \sim 2.2$ factor appropriate for an integrated luminosity of $L = 500\ \mathrm{fb}^{-1}$, the only channel with reasonable error ($\lesssim 15\%$) would be $b\bar{b}$. Further, in obtaining results for ratios of $B(P^0 \to F)$ for $F = gg, b\bar{b}, \tau^+\tau^-$, one must unfold the mis-tagging (implying introduction of systematic uncertainties) and combine statistical errors in the various tagged channels.

The next step, beyond the extraction of ratios of the P^0 branching fractions, is the model-independent determination of the individual $B(P^0 \to F)$'s for specific final states F via the ratio of the rate in a specific final state to the inclusive rate:

$$B(P^0 \to F) = \frac{\sigma(e^+e^- \to \gamma P^0) B(P^0 \to F)}{\sigma(e^+e^- \to \gamma P^0)} . \tag{39}$$

The crucial issue is then the ability to observe the P^0 inclusively in the γX final state as a peak in the recoil M_X spectrum, and the associated error in the inclusive cross section $\sigma(e^+e^- \to \gamma P^0)$. The resolution in M_X is determined by the photon energy resolution. Using $\Delta E_\gamma/E_\gamma = 0.12/\sqrt{E_\gamma} \oplus 0.01$, one finds $\pm 1\sigma$ mass windows in m_{P^0} of $[0,78]$, $[83.5,114]$ and $[193,207]$ (GeV units) for $m_{P^0} = 55$, 100 and 200 GeV, respectively. If the resolution could be improved to $\Delta E_\gamma/E_\gamma = 0.08/\sqrt{E_\gamma} \oplus 0.005$ [38], then the mass windows for $m_{P^0} = 55$, 100 and 200 GeV become $[36,69]$, $[91,108]$ and $[196,204]$, respectively. [We note that $\Delta E_\gamma/E_\gamma \gtrsim 0.0125$ ($\gtrsim 0.0075$) for $m_{P^0} \leq 200$ GeV for the first (second) resolution case, indicating that the constant term is dominant and should be the focus for improving this particular signal.]

Backgrounds to inclusive γP^0 detection will be substantial. All the backgrounds plotted in Fig. 9 must be included (integrated over the appropriate mass window), and others as well. Observation of the P^0 signal in the recoil M_X spectrum would be difficult, especially for lower values of m_{P^0}. However, if m_{P^0} is known ahead of time, then one can simply employ the appropriate mass window and estimate the background from M_X bins outside the mass window. We anticipate that the resulting errors for $\sigma(e^+e^- \to \gamma P^0)$ will be large, implying that the corresponding model-independent determinations of the various $B(P^0 \to F)$'s from Eq. (39) will be subject to large statistical uncertainty. This is an important loss relative to the usual program for determining the properties of a Higgs boson in a model-independent manner using the $e^+e^- \to Zh$ signal in the inclusive $e^+e^- \to ZX$ final state.

Overall, one cannot be optimistic that an e^+e^- collider will provide more than very rough determinations of the fundamental parameters of the effective Lagrangian described earlier. We will now show that prospects at a muon collider are potentially much better, especially if a first signal and approximate mass determination is provided ahead of time by the Tevatron and/or LHC or by an e^+e^- collider.

[7] Note that the reason we focus on ratios is that the systematic errors due to uncertainty in the absolute normalization of the rate in any given channel will cancel out in the ratios.

6 P^0 production at a $\gamma\gamma$ collider

The rate for production and decay of a narrow resonance R in $\gamma\gamma$ collisions is given by [39]

$$N(\gamma\gamma \to R \to F) = \frac{8\pi\Gamma(R \to \gamma\gamma)B(R \to F)}{m_R^2 E_{e^+e^-}} \tan^{-1}\frac{\Gamma_{\rm exp}}{\Gamma_R^{\rm tot}} \left(1 + \langle\lambda\lambda'\rangle\right) G(y_R) L_{e^+e^-}\,, \tag{40}$$

where λ and λ' are the helicities of the colliding photons, $\Gamma_{\rm exp}$ is the mass interval accepted in the final state F and $L_{e^+e^-}$ is the integrated luminosity for the colliding electron and positron beams. In Eq. (40), $\langle\lambda\lambda'\rangle$ and $G(y_R \equiv m_R/E_{e^+e^-})$ depend upon the details of the $\gamma\gamma$ collision set-up. Here, we are interested in exploring the ability of a $\gamma\gamma$ collider to discover the narrow P^0 resonance and so we choose laser polarizations P and P' and e^+e^- beam helicities λ_e and λ_e' in the configuration $2\lambda_e P \sim +1$, $2\lambda_e' P' \sim +1$, $PP' \sim +1$ such that $G \gtrsim 1$ and $\langle\lambda\lambda'\rangle \sim 1$ (which suppresses $\gamma\gamma \to q\overline{q}$ backgrounds) over the large range $0.1 \leq y_R \leq 0.7$. The P^0 is always sufficiently narrow that $\tan^{-1} \to \pi/2$. In this limit, the rate is proportional to $\Gamma(R \to \gamma\gamma)B(R \to F)$. For the P^0, $\Gamma(P^0 \to \gamma\gamma)$ is large and the total production rate will be substantial. In this regard, the importance of the eigenstate composition of the P^0 has already been noted; *e.g.* for the same mass, if the π_D were the mass eigenstate it would have only 1/8 the production rate.

In Fig. 3, we plotted $\Gamma(P^0 \to \gamma\gamma)B(P^0 \to b\overline{b})$ divided by $\Gamma(h \to \gamma\gamma)B(h \to b\overline{b})$, where h denotes the SM Higgs boson. Over the $m_{P^0} = m_h$ range from 15 to 150 GeV, the ratio varies from ~ 8 down to ~ 3, rising to very large values at masses above 160 GeV where the $h \to WW, ZZ$ decay modes open up. Since it is well-established [39, 40, 41] that the SM h can be discovered in this decay mode for $40 \lesssim m_h \lesssim 2m_W$, it is clear that P^0 discovery in the $b\overline{b}$ final state will be possible up to at least 200 GeV, down to $\sim 0.1\sqrt{s} \sim 50$ GeV (at $\sqrt{s} \sim 500$ GeV), below which $G(y)$ starts to get small. Discovery at lower values of m_{P^0} would require lowering the $\sqrt{s}$ of the machine.

In order to quantify these claims slightly further, we have taken the results of Ref. [39] (Fig. 2) for the SM Higgs $b\overline{b}$ signal and the $b\overline{b}$ background rate and multiplied the former by the $\Gamma(\gamma\gamma)B(b\overline{b})$ ratio plotted in Fig. 3 and by the correction factor $\tan^{-1}(\Gamma_{\rm exp}/\Gamma_{P^0}^{\rm tot})/\tan^{-1}(\Gamma_{\rm exp}/\Gamma_h^{\rm tot})$ [see Eq. (40)]. The resulting signal and background rates are plotted in Fig. 12, assuming that $L_{\rm eff} \equiv G(y_{P^0})L_{e^+e^-} = 20~{\rm fb}^{-1}$, independent of m_{P^0}. (As already stated, to achieve $G \gtrsim 1$ at the lowest masses would require lowering the machine energy so that $m_{P^0}/\sqrt{s} > 0.1 - 0.2$.) For the $b\overline{b}$ channel, the signal and background rates plotted give $S/\sqrt{B}$ rising from ~ 8 at $m_{P^0} \sim 20$ GeV to ~ 200 at $m_{P^0} \sim 200$ GeV.

Of course, these results are not entirely realistic. The $\gamma\gamma \to b\overline{b}$ background rate plotted assumes an unrealistically small $b\overline{b}$ mass resolution of $\Gamma_{\rm exp} = 5$ GeV. In addition, backgrounds from $\gamma\gamma \to c\overline{c}g$ and $\gamma\gamma \to b\overline{b}g$ are ignored. (These are not suppressed by having $\langle\lambda\lambda'\rangle \sim 1$.) However, these three-jet backgrounds can be largely eliminated by using topological tagging and cuts designed to isolate the two-

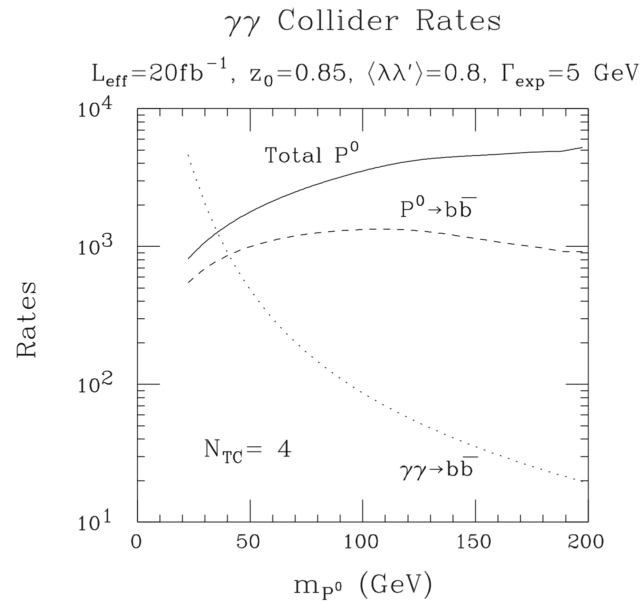

Figure 12: We consider $\gamma\gamma$ collisions for $L_{\rm eff} = 20$ fb^{-1} (assumed independent of m_{P^0}), with an angular cut of $|\cos\theta| < 0.85$ applied to the two-particle final state. An experimental resolution $\Gamma_{\rm exp} = 5$ GeV is assumed in the final state. We plot, as a function of m_{P^0}: the total $\gamma\gamma \to P^0$ production rate (solid); the rate for $\gamma\gamma \to P^0 \to b\overline{b}$ (dashes); and the $\gamma\gamma \to b\overline{b}$ irreducible background rate (dots). $N_{TC} = 4$ is assumed.

jet final state. The resulting additional efficiency reduction for the $P^0 \to b\bar{b}$ signal is typically no smaller than $\gtrsim 0.5$ (for single-b topological tagging) [41]. Thus, P^0 discovery at a $\gamma\gamma$ collider in the $b\bar{b}$ final state will be very viable over a large mass range.

Once the P^0 has been discovered, either in $\gamma\gamma$ collisions or elsewhere, one can configure the $\gamma\gamma$ collision set-up so that the luminosity is peaked at $\sqrt{s}_{\gamma\gamma} \sim m_{P^0}$. A very precise measurements of the the P^0 rate in the $b\bar{b}$ final state will then be possible. For example, rescaling the SM Higgs 'single-tag' results of Table 1 of Ref. [41] (which assumes a peaked luminosity distribution with a total of $L = 10$ fb^{-1}) for the 106 GeV $\leq m_{jj} \leq$ 126 GeV mass window to the case of the P^0 using the ratio plotted in Fig. 3, we obtain $S \sim 5640$ compared to $B \sim 325$, after angular, topological tagging and jet cuts. This implies a statistical error for measuring $\Gamma(P^0 \to \gamma\gamma)B(P^0 \to b\bar{b})$ of $\lesssim 1.5\%$. Systematic errors will probably dominate.

Of course, it would be very interesting to measure rates in other final state channels as well. The total P^0 rate shown in Fig. 12 (which can be further increased once m_{P^0} is known and the $\gamma\gamma$ collisions are configured for a peaked, rather than broad, luminosity spectrum) indicates that $\gamma\gamma \to P^0 \to \tau^+\tau^-$ and gg will also have large event rates. Backgrounds are probably too large in the gg final state to obtain a robust P^0 signal. Backgrounds in the $\tau^+\tau^-$ channel are not a large, but there is no sharp mass peak in this channel. Still, if one configures the machine energy and $\gamma\gamma$ collision set-up so that the $\gamma\gamma$ luminosity is very peaked at an already known value of m_{P^0}, a reasonably precise measurement of $\Gamma(P^0 \to \gamma\gamma)B(P^0 \to \tau^+\tau^-)$ might prove possible. Detailed studies of what can be achieved in the gg and $\tau^+\tau^-$ channels should be performed.

It might even be possible to detect the P^0 in the $\gamma\gamma \to P^0 \to \gamma\gamma$ mode. The (broad-luminosity-profile) total P^0 production rate plotted in Fig. 12 is > 3500 for $m_{P^0} > 100$ GeV, for which masses $B(P^0 \to \gamma\gamma) > 0.006$ (Fig. 1). The resulting total $\gamma\gamma \to P^0 \to \gamma\gamma$ event rate ranges from a low of ~ 20 at $m_{P^0} \sim 100$ GeV to ~ 50 at $m_{P^0} \sim 200$ GeV. These rates can be substantially increased if the $\gamma\gamma$ collision set-up is optimized for a known value of m_{P^0}. Presumably the (one-loop) irreducible $\gamma\gamma \to \gamma\gamma$ background is quite small. But, one must worry about jets that fake photons and possibly about back-scattered photons that simply pass through into the final state without interacting. (Presumably a minimum-angle cut could be used to largely eliminate the latter.) Once again, a detailed study will be needed to reliably assess prospects for detection of the $P^0 \to \gamma\gamma$ signal.

7 P^0 production at a muon collider

In this section, we consider s-channel production of the P^0 at a future $\mu^+\mu^-$ collider. Given the mass eigenstate compositions of Eq. (7) [see also Eqs. (15) and (16)] it is only the P^0, and not the $P^{0\prime}$, that has tree-level coupling to $\mu^+\mu^-$. The s-channel production rate for the $P^{0\prime}$ via its one-loop-induced coupling to $\mu^+\mu^-$ will generally be much smaller than the tree-level s-channel production rate for the P^0 so long as there is no fine-tuned cancellation between $m_4^{(2)}$ and $m_{10}^{(2)}$ in the expression for λ_μ, Eq. (24). Our discussion will expand on the results of Ref. [27]. Related work can be found in Ref. [42]. As in previous sections, we shall employ the specific P^0 properties as predicted by the couplings of Eq. (27), (29) and (32). However, the general features of our results will apply in a broad sense to other choices for the fermionic couplings and to other models of a strongly interacting electroweak sector.

We have already noted that for $\Lambda < 10$ TeV, $m_{P^0}(\mathrm{one-loop})$ will be smaller than m_Z. Thus, as in earlier sections, it is important to consider small masses as well as masses up to the maximum 200 GeV value considered in this paper. For much of this mass range a muon collider would provide an excellent probe of the P^0 via the direct s-channel production process $\mu^+\mu^- \to P^0$. The basic reasons as to why this is so are the following. First, the P^0 has a sizeable $\mu^+\mu^-$ coupling [Eq. (27)]. Second, the muon collider has the (unique) ability to achieve a very narrow Gaussian spread, $\sigma_{\sqrt{s}}$, in $\sqrt{s}$, as necessary to obtain a large P^0 cross section given the very narrow width of the P^0 (as plotted in Fig. 2). Indeed, one can achieve $R = 0.003\%$ beam energy resolution with reasonable luminosity at the muon collider, leading to

$$\sigma_{\sqrt{s}} \sim 1 \text{ MeV} \left(\frac{R}{0.003\%}\right)\left(\frac{\sqrt{s}}{50 \text{ GeV}}\right) . \tag{41}$$

In addition, the beam energy can be very precisely tuned ($\Delta E_{\rm beam} \sim 10^{-6}$ is achievable [44]) as is crucial in scanning for a resonance with a width as small as that predicted for the P^0.

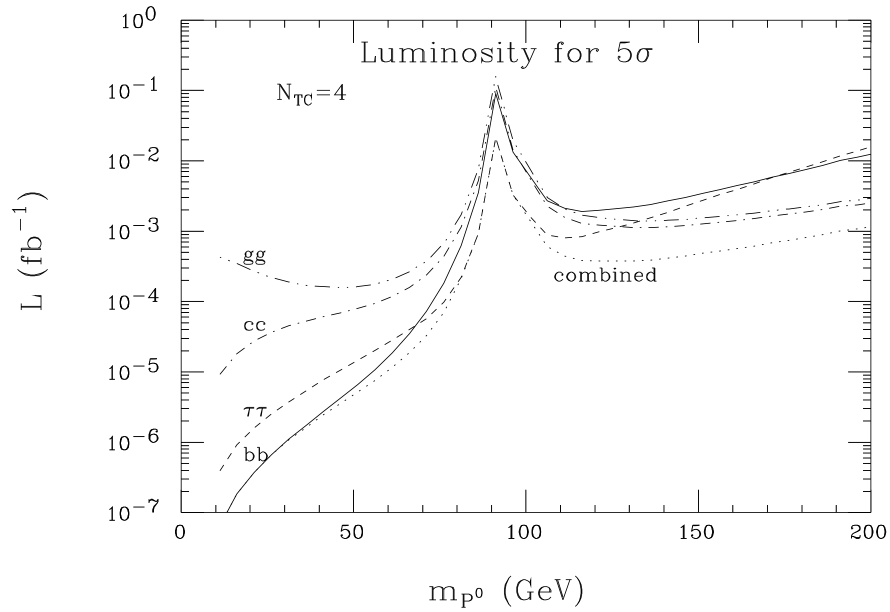

Figure 13: Luminosity required for a $S/\sqrt{B} = 5$ signal for the P^0 in various 'tagged' channels ($b\overline{b}$, $\tau^+\tau^-$, $c\overline{c}$, gg) and for the optimal combination of these four channels.

To quantitatively assess the ability of the muon collider to discover the P^0 we have proceeded as follows. We compute the P^0 cross section by integrating over the resonance using a $\sqrt{s}$ distribution given by a Gaussian of width $\sigma_{\sqrt{s}}$ (using $R = 0.003\%$) modified by bremsstrahlung photon emission. (Beamstrahlung is negligible at a muon collider.) See Ref. [45] for more details. We separate $b\overline{b}$, $\tau^+\tau^-$, $c\overline{c}$ and $q\overline{q}/gg$ final states by using topological and τ tagging with efficiencies and mis-tagging probabilities as estimated by B. King [37]. These were summarized in the previous section and used for our e^+e^- collider discussion. Further, only events in which the jets or τ's have $|\cos\theta| < 0.94$ (corresponding to a nose cone of 20°) are considered. As in the e^+e^- collider study, a jet final state is deemed to be: $b\overline{b}$ if one or more jets is tagged as a b; $c\overline{c}$ if no jet is tagged as a b, but one or more jets is tagged as a c; and $q\overline{q}/gg$ if neither jet is tagged as a b or a c. Background and signal events are analyzed in exactly the same manner.

In Fig. 13, we plot the integrated luminosity required to achieve $S_i/\sqrt{B_i} = 5$ in a given channel, i (as defined after tagging), taking $\sqrt{s} = m_{P^0}$. We also show the luminosity L needed for $\sum_k S_k/\sqrt{\sum_k B_k} = 5$, where the optimal choice of channels k is determined for each m_{P^0}. We observe that very modest L is needed unless $m_{P^0} \sim m_Z$.

7.1 Scanning and Centering

Of course, luminosity must be devoted to scanning for the P^0 if it has not yet been discovered or to centering on $\sqrt{s} \simeq m_{P^0}$ assuming that m_{P^0} has been measured up to a certain level of uncertainty at another type of accelerator. As we have discussed, the P^0 is very likely to have been discovered at the LHC in the $gg \to P^0 \to \gamma\gamma$ mode if $m_{P^0} > 50$ GeV or so. If it is observed in this mode, then its mass will be very accurately measured, almost certainly to better than $\Delta m \sim 100$ MeV. We have also seen that for $m_{P^0} < 50$ GeV, discovery or exclusion at the $N_{SD} = 3$ level, or better, will be possible using the $e^+e^- \to \gamma P^0$ mode. However, the mass uncertainty associated with P^0 observation in $e^+e^- \to \gamma P^0$ collisions will be much larger — $\Delta m >$ few GeV is likely.

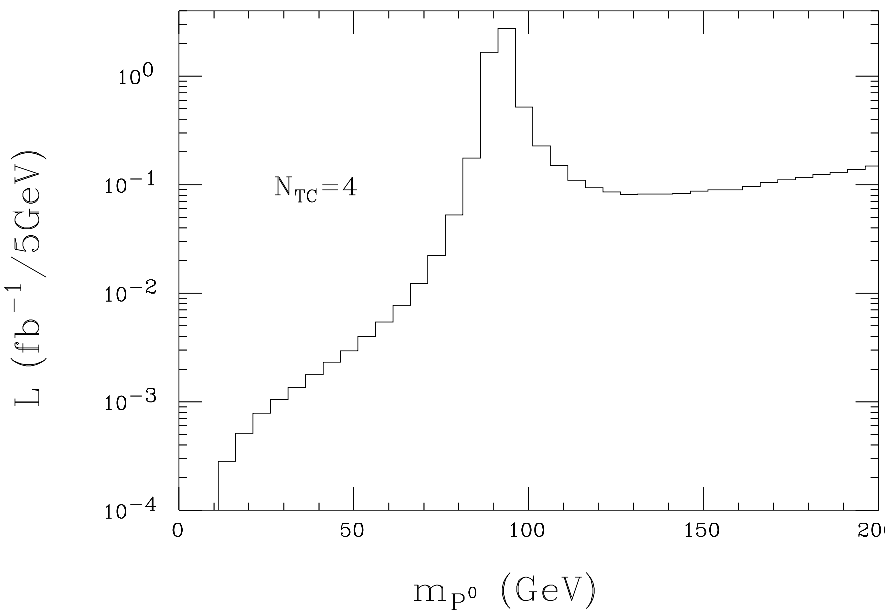

Figure 14: Maximum luminosity needed to either discover or exclude the P^0 at the $S/\sqrt{B} = 3$ level by scanning in various 5 GeV intervals, based on using the optimal combination of channels (as defined by the tagging probabilities given in the text).

To estimate the luminosity required at the muon collider for scanning a given interval so as to either discover or eliminate the P^0, we have adopted the following approach. We imagine choosing $\sqrt{s}$ values separated by $2\sigma_{\sqrt{s}}$. We assume the worst case scenario in which the resonance sits midway between the two $\sqrt{s}$ values. The signal and (separately) background rates for these two $\sqrt{s}$ values are summed together (for the optimal channel combination) and the net $N_{SD} \equiv (S_1 + S_2)/(B_1 + B_2)^{1/2}$ is computed. We require $N_{SD} = 3$ to claim a signal. The luminosity required for a successful scan of a given interval is computed assuming that the resonance lies between the last two scan points. This, in combination with the fact that $\sigma_{\sqrt{s}}$ for $R = 0.003\%$ is typically a factor of two smaller than $\Gamma^{\rm tot}_{P^0}$ (implying that points further away than $\sigma_{\sqrt{s}}$ from the resonance could be usefully included in establishing a signal) will imply that the integrated luminosities we compute in this way are quite conservative. It is important to note that if a signal is seen for the P^0 in the above-described scanning procedure, then m_{P^0} will be determined to within $\lesssim \sigma_{\sqrt{s}}$; in addition, we will obtain a first rough measurement of $\Gamma^{\rm tot}_{P^0}$.

In Fig. 14, we give the integrated luminosity required to either discover or exclude the P^0 at the $N_{SD} = 3$ level after scanning the indicated 5 GeV intervals, assuming that m_{P^0} lies within that interval. As expected, rather modest luminosity is required except for intervals near the peak in the background at $\sqrt{s} \sim m_Z$ due to the $\mu^+\mu^- \to Z$ process.

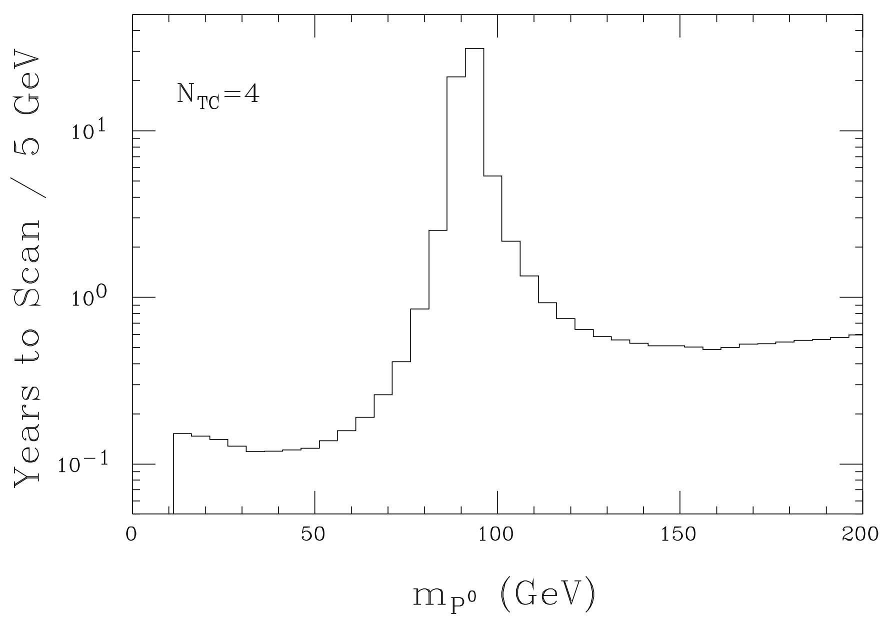

Figure 15: The number of years required to either discover or exclude the P^0 at the $S/\sqrt{B} = 3$ level by scanning in various 5 GeV intervals, based on the results of Fig. 14 and assuming luminosity as given in Eq. (42).

To assess the implications of Fig. 14, we must discuss the luminosity that will be available at a $\mu^+\mu^-$ collider as a function of $\sqrt{s}$. We will do so assuming that the first muon collider is designed for optimum performance at $\sqrt{s} \sim 100$ GeV, and that for $R = 0.003\%$ a yearly integrated luminosity of $L = 0.1$ fb^{-1} can be achieved [46]. For energies on either side of $\sqrt{s} = 100$ GeV, the integrated luminosity will vary according to [46]:

$$
\begin{aligned}
L_{\rm year} &= 0.1 \text{ fb}^{-1} \left(\frac{\sqrt{s}}{100 \text{ GeV}} \right)^2 , \quad \sqrt{s} < 100 \text{ GeV} , \\
L_{\rm year} &= 0.1 \text{ fb}^{-1} \left(\frac{\sqrt{s}}{100 \text{ GeV}} \right)^{4/3} , \quad \sqrt{s} > 100 \text{ GeV} . \qquad (42)
\end{aligned}
$$

Using these expectations, we can determine the maximum (given the rather pessimistic assumptions employed for the scan) number of years of operation required to scan each of the 5 GeV intervals of Fig. 14 and either exclude or discover the P^0 at the $N_{SD} = 3$ level. The results are plotted in Fig. 15. We note that at most ~ 3 years would be required to scan the entire range of $m_{P^0} < 80$ GeV in which m_{P^0} is expected to lie if one-loop mass contributions are dominant and assuming $\Lambda < 10$ TeV. However, should m_{P^0} be near m_Z, then prior discovery of the P^0 at another accelerator will be crucial in order that we be able to center on $\sqrt{s} \sim m_{P^0}$ and perform detailed studies.

From our earlier discussions, such prior discovery at the LHC appears to be quite likely if $m_{P^0} > 50$ GeV (possibly lower, pending a detailed study), and will result in mass uncertainty of less than $\Delta m \sim 100$ MeV. Prior discovery at an e^+e^- collider is also reasonably likely if $m_{P^0} \lesssim 50$ GeV, although the mass uncertainty will be much larger, $\Delta m \sim$ few GeV. The very worst case, and one for which LHC discovery will provide vital input, is $m_{P^0} \simeq m_Z$. For this case, about 0.016 fb^{-1} (see Fig. 13, optimal channel combination) would be required to exclude or detect the P^0 at the N_{SD} level at each of $\sim 100\ \mathrm{MeV}/\sigma_{\sqrt{s}} = 25$ points separated by $2\sigma_{\sqrt{s}} \sim 4$ MeV. At most, this would require about 1/2 year of collider operation, assuming $L \sim 0.1\ \mathrm{fb}^{-1}$ per year at $\sqrt{s} \sim m_Z$. Conversely, without the LHC input we would be very lucky to find the P^0 by scanning at the muon collider when $m_{P^0} \sim m_Z$.

Let us next suppose that $m_{P^0} < 50$ GeV and that the LHC does not discover the P^0. However, let us assume that an e^+e^- collider does discover the P^0 and measures m_{P^0} to within (to be on the pessimistic side) $\Delta m \sim 5$ GeV. From Fig. 15, we see that no more than ~ 0.15 years is required to scan any 5 GeV interval in the $m_{P^0} < 50$ GeV range so as to discover and center on $\sqrt{s} \simeq m_{P^0}$ within $< \sigma_{\sqrt{s}}$.

Overall, it will very probably be possible to center on $\sqrt{s} \simeq m_{P^0}$ at a muon collider in significantly less than a year of operation. Once centered, the important question is how well we will be able to determine the 6 m_i parameters of the effective Yukawa Lagrangian [see Eq. (6)] associated with the $T_3 = -1/2$ sector — m_2', m_4, $m_4^{(2)}$, m_9, m_{10} and $m_{10}^{(2)}$ — and the value of N_{TC}. All of these go into determining the properties of the P^0 in production and decay and are potentially measurable if enough accurate experimental input is available. In order to assess the situation in this regard, we must first determine the accuracy with which the basic experimental observables can be measured.

7.2 Precision Measurements

At the muon collider, the quantities that we can hope to measure with precision are the rates in the various tagged channels and the total width of the P^0. This set of observables is the same as for the SM Higgs boson, for which the procedures have been studied and discussed in detail in Ref. [45]. We will follow very similar procedures here. In particular, for the determination of $\Gamma_{P^0}^{\mathrm{tot}}$ we employ the optimized three-point scan described in Ref. [45] in which luminosity of amount L_1 is employed at $\sqrt{s} \simeq m_{P^0}$ and of amounts $2L_1$ at each of the two points $\sqrt{s} \simeq m_{P^0} \pm 2\sigma_{\sqrt{s}}$, implying a total luminosity for the scan of $5L_1$. We will assume that 4 years of running at $R = 0.003\%$ is employed for the three-point scan, corresponding to a total integrated luminosity of $5L_1$ equal to 4 times the yearly luminosity given in Eq. (42). The equivalent luminosity that would have to be expended at $\sqrt{s} \simeq m_{P^0}$ in order to obtain the same statistics for the various channel rate measurements is about 3/4 of the L employed for the scan. (This is a somewhat larger fraction than in the Higgs case due to the fact that, for the parameters chosen, $\Gamma^{\rm tot}_{P^0}$ is significantly larger than the Higgs width at the same mass.) In other words, the statistics for the channel rates will be approximately the same as obtained if L equal to 3 times the yearly luminosity of Eq. (42) is accumulated at $\sqrt{s} \simeq m_{P^0}$.

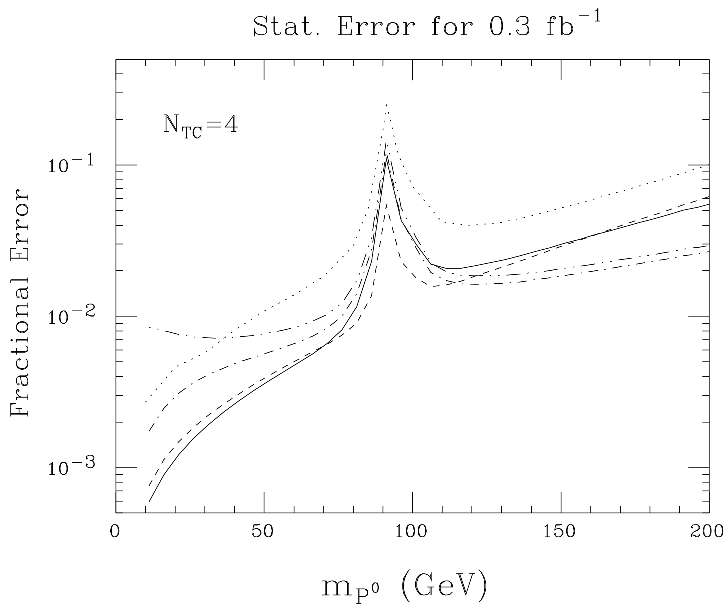

Figure 16: The fractional statistical error for the various tagged channel rates obtained if $L = 0.3$ fb^{-1} is accumulated (with $R = 0.003\%$) at $\sqrt{s} \simeq m_{P^0}$. Also shown is the error for $\Gamma^{\rm tot}_{P^0}$ obtained using the optimal three-point scan and $L = 0.4$ fb^{-1}. Curve notation is: $b\overline{b}$ (solid); $\tau^+\tau^-$ (dashes); $c\overline{c}$ (dot-dash); gg (dot-dot-dash); $\Gamma^{\rm tot}_{P^0}$ (dots).

The only difference in our optimal three-point scan procedures for determining $\Gamma^{\rm tot}_{P^0}$ as compared to the Higgs boson case is the following. At each m_{P^0}, we compute the error in $\Gamma^{\rm tot}_{P^0}$ by using the total signal $S = \sum_k S_k$ and background $B = \sum_k B_k$ rates for the combination of channels k which gives the largest net $S/\sqrt{B}$, as described earlier.

We begin by plotting in Fig. 16 the statistical errors for the $b\overline{b}$, $\tau^+\tau^-$, $c\overline{c}$ and gg channel rates using the channel identification (and mis-identification) efficiencies quoted earlier, assuming that $L = 0.3$ fb^{-1} is accumulated at $\sqrt{s} \simeq m_{P^0}$. Also shown is the result for the error in the total width obtained for $L = 0.4$ fb^{-1} by employing

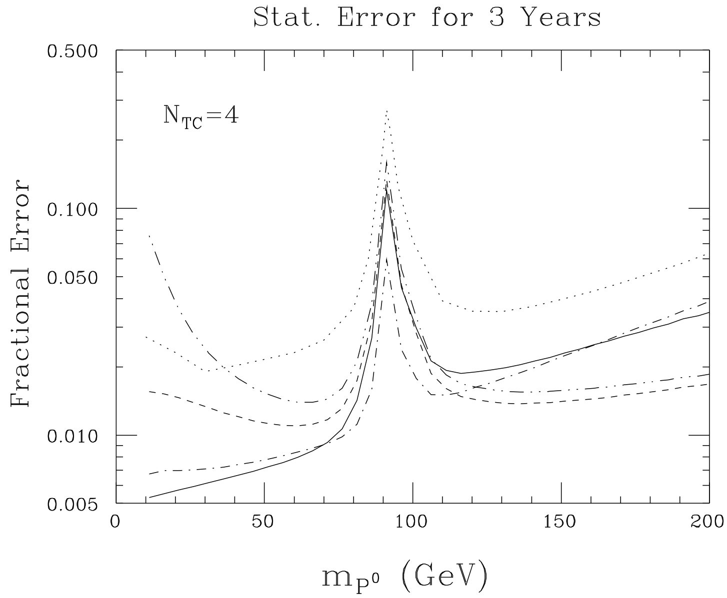

Figure 17: The fractional statistical error for the various tagged channel rates obtained after 3 years of operation at $\sqrt{s} \simeq m_{P^0}$ or, equivalently, after 4 years of running devoted to the optimal three-point scan, assuming yearly luminosity as given in Eq. (42) at $R = 0.003\%$. Also shown is the fractional error for $\Gamma^{\rm tot}_{P^0}$ obtained after devoting 4 years to the optimal three-point scan. Curve notation is: $b\overline{b}$ (solid); $\tau^+\tau^-$ (dashes); $c\overline{c}$ (dot-dash); gg (dot-dot-dash); $\Gamma^{\rm tot}_{P^0}$ (dots).

the optimal three-point scan procedure. (As noted earlier, the $L = 0.4$ fb^{-1} scan gives approximately the same statistics for the channel rates as does $L = 0.3$ fb^{-1} sitting on-resonance, $\sqrt{s} \simeq m_{P^0}$.)

These errors must be adjusted for the fact that the machine luminosity is a variable function of $\sqrt{s}$. Thus, in Fig. 17 we plot the tagged channel fractional statistical errors assuming 3 years of running at $\sqrt{s} \simeq m_{P^0}$ with luminosity given by Eq. (42). As described earlier, these errors are approximately the same as would be achieved after devoting 4 years of machine operation to the optimal three-point scan of the P^0 resonance. Also shown is the result for the $\Gamma^{\rm tot}_{P^0}$ error if 4 years of running with yearly luminosity as given in Eq. (42) is devoted to the three-point optimal scan. The resulting errors are encouragingly small.

8 Determining the Parameters of the Model

In the previous sections, we have described the experimental information, and associated statistical errors, that will probably become available regarding the P^0. We now consider the strategy for using this experimental information to extract the underlying parameters of the model.

Let us first consider the limit in which the various probabilities for channel identification and mis-identification are precisely known and, in addition, uncertainty arising from the absolute normalization of event rates is small. In this limit, the errors for the various quantities we consider are purely statistical. In practice, additional contributions to the errors for the model parameters will arise from systematic errors associated with the determination of the channel tagging and mis-tagging probabilities (by simulation and experimental studies) and overall event rate normalization. However, without a detailed detector scenario and study, we cannot assess the level of the systematic errors that will arise.

The experimentally well-measured quantities that could be available to us are:

- $\Gamma_{P^0}^{\rm tot}$ from the muon collider;
- $\Gamma(P^0 \to gg)B(P^0 \to \gamma\gamma)$ from the LHC;
- $\Gamma(P^0 \to \gamma\gamma)B(P^0 \to b\bar{b})$ from the $\gamma\gamma$ collider; and
- $\Gamma(P^0 \to \mu^+\mu^-)B(P^0 \to F)$ for $F = b\bar{b}, \tau^+\tau^-, gg$ from the muon collider (after unfolding the channel mis-identification).

We have discounted the e^+e^- data because of the very large errors that are anticipated; see Fig. 11. Using the measured value of $\Gamma_{P^0}^{\rm tot}$, we can convert the second, third and fourth items of the above list into results for $\Gamma(P^0 \to gg)\Gamma(P^0 \to \gamma\gamma)$, $\Gamma(P^0 \to \gamma\gamma)\Gamma(P^0 \to b\bar{b})$ and $\Gamma(P^0 \to \mu^+\mu^-)\Gamma(P^0 \to F)$ ($F = b\bar{b}, \tau^+\tau^-, gg$), respectively.

If we employ the constraints on the parameters deriving from the quark and lepton masses, Eq. (9), then the experimentally measured quantities listed have the following reduced parameter dependences:

$$\Gamma(P^0 \to gg)\Gamma(P^0 \to \gamma\gamma) \propto \frac{N_{TC}^4}{v^4}\,; \tag{43}$$

$$\Gamma(P^0 \to \gamma\gamma)\Gamma(P^0 \to b\bar{b}) \propto \frac{N_{TC}^2}{v^2}\left[4m_2' - 3m_b\right]^2\,; \tag{44}$$

$$\Gamma(P^0 \to \mu^+\mu^-)\Gamma(P^0 \to b\bar{b}) \propto \left[\frac{4}{3}m_4^{(2)} - \frac{1}{3}m_\mu\right]^2 \left[4m_2' - 3m_b\right]^2\,; \tag{45}$$

$$\Gamma(P^0 \to \mu^+\mu^-)\Gamma(P^0 \to \tau^+\tau^-) \propto \left[\frac{4}{3}m_4^{(2)} - \frac{1}{3}m_\mu\right]^2 \left[\frac{4}{3}m_4 - \frac{1}{3}m_\tau\right]^2\,; \tag{46}$$

$$\Gamma(P^0 \to \mu^+\mu^-)\Gamma(P^0 \to gg) \propto \left[\frac{4}{3}m_4^{(2)} - \frac{1}{3}m_\mu\right]^2 \frac{N_{TC}^2}{v^2}\,. \tag{47}$$

The following strategy then emerges.

- Determine N_{TC}/v from Eq. (43);
- Determine $|4m_2' - 3m_b|$ from N_{TC}/v and Eq. (44);

- Determine $|\frac{4}{3}m_4^{(2)} - \frac{1}{3}m_\mu|$ from N_{TC}/v and Eq. (47);
- Determine $|\frac{4}{3}m_4 - \frac{1}{3}m_\tau|$ from $|\frac{4}{3}m_4^{(2)} - \frac{1}{3}m_\mu|$, N_{TC}/v and Eq. (46);
- Determine $|4m_2' - 3m_b|$ from $|\frac{4}{3}m_4^{(2)} - \frac{1}{3}m_\mu|$, N_{TC}/v and Eq. (45).

Note that the $\gamma\gamma$ collider measurement allows a consistency cross check, which amounts to checking that the formulas for the ggP^0 and $\gamma\gamma P^0$ anomalous couplings are both correct. Assuming no inconsistencies, we would be left with two-fold ambiguities for $m_4^{(2)}$, m_4 and m_2'. For each of the eight choices, we may proceed as follows:

- Determine m_9, m_{10} and $m_{10}^{(2)}$ from m_2', m_4 and $m_4^{(2)}$ using Eq. (9);
- Compute ρ_8 using Eq. (12);
- Compute a 'one-loop value' for Λ/v using ρ_8 and Eq. (11).

The assumption of a generation-independent relation between the leptonic couplings of the P^0 and the lepton masses would imply that the m_4 and $m_4^{(2)}$ solutions should have the same relation to the corresponding lepton masses, thereby reducing the potential eight-fold ambiguity to a four-fold ambiguity. Experimentally, if there are solutions consistent with generation-independence it would be hard to imagine that nature has not made this choice. It is only if there are no solutions that allow generation-independent couplings that one will feel forced to consider the full set of ambiguities.

In the context of the present model, $v = 246$ GeV and the above (unambiguous) determination of N_{TC}/v would then yield a result for N_{TC}. A solution-case-dependent value for the one-loop cutoff Λ (that would apply if LQ mass-squared contributions are small) would also be obtained. In a more general walking technicolor model, the effective value of v could, however, be different.

One could also ask how consistent each of the solutions is with the LQ mass-squared contributions being small in comparison to one-loop Yukawa contributions. An example of how this might proceed is provided by the sample parameter choices of Eq. (25), which yields $\rho_8 = \frac{1}{2}(m_b^2 - m_\tau^2)$ (neglecting the $-\frac{1}{2}m_\mu^2$ contribution). The alternative m_i choices giving the same values of $|\frac{4}{3}m_4^{(2)} - \frac{1}{3}m_\mu|$, $|\frac{4}{3}m_4 - \frac{1}{3}m_\tau|$ and $|4m_2' - 3m_b|$, while maintaining consistency with Eq. (9), are:

$$(m_2' = m_b, m_9 = 0)\,; \quad (m_4 = m_\tau, m_{10} = 0)\,; \quad \text{and/or} \quad (m_4^{(2)} = m_\mu, m_{10}^{(2)} = 0)\,. \tag{48}$$

The alternative values that emerge for ρ_8 are: (1) 0 for $m_9 = m_{10} = 0$; (2) $\frac{1}{2}m_b^2$ for $m_9 = m_b/2$ and $m_{10} = 0$; and (3) $-\frac{1}{2}m_\tau^2$ for $m_9 = 0$ and $m_{10} = m_\tau/2$. Of these, (1) and (3) are clearly unphysical. Thus, if LQ contributions to the mass-squared matrix are not substantial, the only physically consistent value of (m_2', m_9) would be $(\frac{1}{2}m_b, \frac{1}{2}m_b)$, and (keeping generation universality for the leptonic couplings) the only ambiguity would be between the choices $(m_4, m_{10}) = (-m_\tau/2, m_\tau/2)$, $(m_4^{(2)}, m_{10}^{(2)}) = (-m_\mu/2, m_\mu/2)$ vs. $(m_4, m_{10}) = (m_\tau, 0)$, $(m_4^{(2)}, m_{10}^{(2)}) = (m_\mu, 0)$.

Whether or not we pursue this last strategy that assumes one-loop dominance of the mass-squared matrix, we see that a detailed study of the P^0 would provide a lot of information about the low-energy effective Lagrangian of the model.

Let us now consider the errors that will arise in the determination of the parameters through the above equations, given the statistical errors plotted in Figs. 4 and 17 and noted for the $\gamma\gamma$ collider. We have seen that the statistical errors for the CMS measurement of $\Gamma(P^0 \to gg)B(P^0 \to \gamma\gamma)$ and the $\gamma\gamma$-collider measurement of $\Gamma(P^0 \to \gamma\gamma)B(P^0 \to b\bar{b})$ will be at the $1-2\%$ level. In considering the statistical errors for the tagged channel rates plotted in Fig. 17, we must recall that the rate for a given tagged channel F is, to a good approximation, proportional to $\sum_X \Gamma(P^0 \to \mu^+\mu^-)B(P^0 \to X)\epsilon_{X/F}$, where the $\epsilon_{X/F}$ are the probabilities (detailed earlier) that a channel X is identified as channel F. Thus, a certain amount of unfolding will be required to get to the rates for the true channels. As discussed earlier, there will be systematic errors associated with this process. In addition, there will be systematic errors coming from uncertainties in the overall absolute rate in the $gg \to P^0 \to \gamma\gamma$ CMS measurement of $\Gamma(P^0 \to gg)B(P^0 \to \gamma\gamma)$, in the absolute rate for the $\gamma\gamma$-collider measurement of $\Gamma(P^0 \to \gamma\gamma)B(P^0 \to b\bar{b})$ and in the overall absolute rate for P^0 production in the sum of all channels at the muon collider. It is hard to imagine that these systematic errors will be smaller than $\sim 10\%$. Given that the statistical errors are, for the most part (*i.e.* except if $m_{P^0} \sim m_Z$) much smaller than 10%, there is little point in doing a detailed error analysis until the muon-collider systematic errors can be better estimated on the basis of a detailed muon-collider detector design. If the systematic errors are of order 10%, the parameters of the model (for any one of the choices consistent with the experimental determinations of $|\frac{4}{3}m_4^{(2)} - \frac{1}{3}m_\mu|$, $|\frac{4}{3}m_4 - \frac{1}{3}m_\tau|$ and $|4m_2' - 3m_b|$) will have systematic errors that are somewhat larger, perhaps 15%–20%. We also note that if the systematic errors cannot be brought below the 10% level, then one could devote less than 4 years of muon collider running time to the optimal three-point scan without significantly impacting the overall errors for the model parameters.

9 Conclusion

In this paper, we have considered the production and study of the lightest pseudo-Nambu Goldstone state (denoted P^0) of a typical technicolor model at future pp, e^+e^- and $\mu^+\mu^-$ colliders. In the broad class of models considered, the P^0 is of particular interest because it contains only down-type techniquarks (and charged technileptons) and thus will have a mass scale that is most naturally set by the mass of the b-quark. Other color-singlet PNGB's will have masses most naturally set by m_t, while color non-singlet PNGB's will generally be even heavier. Vector resonance states such as the technirho and techniomega are likely to be heavier still. Thus, it is of great importance to understand what the prospects for discovering the P^0 are and whether we can study its properties in enough detail to determine key features and parameters of the technicolor model. We have focused our study on the m_{P^0} mass range that is typically suggested by technicolor models, 10 GeV $< m_{P^0} <$ 200 GeV, and assumed a moderate value for the number of technicolors, $N_{TC} = 4$.

We have found that discovery of the P^0 in the $gg \to P^0 \to \gamma\gamma$ mode at the LHC will almost certainly be possible unless its mass is either very small ($\lesssim$ 30 GeV?) or very large ($\gtrsim$ 200 GeV?), where the question marks are related to uncertainties in LHC backgrounds in the inclusive $\gamma\gamma$ channel. In addition, over much of this mass range, the rate in this channel (which is typically much larger than would arise for a SM Higgs boson) will be measured with very high statistical accuracy ($\lesssim \pm 1\%$, *i.e.* such that systematic uncertainty in the overall rate will dominate). The $gg \to P^0 \to \gamma\gamma$ mode is also predicted to be viable, although over a smaller mass range, at the Tevatron. For the integrated luminosity of TeV33, a reasonably precise ($\lesssim \pm 10\%$) determination of the signal rate will typically be possible for m_{P^0} values such that discovery during RunII is possible. RunI data can already be used to exclude a P^0 in the $50-200$ GeV mass range for $N_{TC} > 12-16$.

In contrast, an e^+e^- collider, while able to discover the P^0 via $e^+e^- \to \gamma P^0$, so long as m_{P^0} is not close to m_Z, is unlikely (unless the TESLA 500 fb^{-1} per year option is built or N_{TC} is very large) to be able to determine the rates for individual γF final states ($F = b\overline{b}, \tau^+\tau^-, gg$ being the dominant P^0 decay modes) with sufficient accuracy as to yield more than very rough indications regarding the important parameters of the technicolor model.

The $\gamma\gamma$ collider option at an e^+e^- collider is actually a more robust means for discovering the P^0 than direct operation in the e^+e^- collision mode. We find that $\gamma\gamma \to P^0 \to b\overline{b}$ should yield an easily detectable P^0 signal for $0.1 \lesssim \frac{m_{P0}}{\sqrt{s}} \lesssim 0.7$ when the $\gamma\gamma$ collision set-up is chosen to yield a broad luminosity distribution. Once m_{P^0} is known, the $\gamma\gamma$ collision set-up can be re-configured to yield a luminosity distribution that is strongly peaked at $\sqrt{s}_{\gamma\gamma} \sim m_{P^0}$ and, for much of the mass range of $m_{P^0} \lesssim$ 200 GeV, a measurement of $\Gamma(P^0 \to \gamma\gamma)B(P^0 \to b\overline{b})$ can be made with statistical accuracy in the $\lesssim 2\%$ range. More detailed studies will be required to determine what is possible in the $P^0 \to gg$, $\tau^+\tau^-$ and $\gamma\gamma$ final states.

A $\mu^+\mu^-$ collider would play a very special role with regard to determining key properties of the P^0. In particular, the P^0, being comprised of $D\overline{D}$ and $E\overline{E}$ techniquarks, will naturally have couplings to the down-type quarks and charged leptons of the SM. Thus, s-channel production ($\mu^+\mu^- \to P^0$) is predicted to have a substantial rate for $\sqrt{s} \sim m_{P^0}$. Because the P^0 has a very narrow width (not much larger than that of a SM Higgs boson of the same mass, assuming a moderate value of N_{TC}), in order to maximize this rate it is important that one operates the $\mu^+\mu^-$ collider so as to have extremely small beam energy spread; $R = 0.003\%$ can be achieved and is very crucial to the conclusions stated below. For this R, the resolution in $\sqrt{s}$ of the muon collider, $\sigma_{\sqrt{s}}$, is of order $\sigma_{\sqrt{s}} \sim 1$ MeV$(\sqrt{s}/50$ GeV$)$, whereas the P^0 width varies from 0.3 MeV to 26 MeV as m_{P^0} ranges from 10 GeV up to 200 GeV (for the particular choice of model parameters that we have employed). Thus, $\sigma_{\sqrt{s}} < \Gamma_{P^0}^{\rm tot}$ is possible and leads to very high P^0 production rates for typical $\mu^+\mu^- \to P^0$ coupling strength. We, of course, have employed the luminosity that is currently anticipated to be achievable (as a function of $\sqrt{s}$) for this R.

Assuming that the P^0 is discovered at the Tevatron, the LHC or (as might be the only possibility if m_{P^0} is very small) at an e^+e^- collider (possibly operating in the $\gamma\gamma$ collider mode), the $\mu^+\mu^-$ collider could quickly (in less than a year) scan the mass range indicated by the previous discovery (for the expected uncertainty in the mass determination) and center on $\sqrt{s} \simeq m_{P^0}$ to within $< \sigma_{\sqrt{s}}$. We then imagine devoting a period of several years to the optimal three-point scan (see main text) of the P^0 resonance in order to determine with high statistical precision all the $\mu^+\mu^- \to P^0 \to F$ channel rates and the total width $\Gamma_{P^0}^{\rm tot}$. For the particular technicolor model parameters we have chosen, 4 years devoted to the scan would yield statistical precisions well-below 10% when m_{P^0} is not close to m_Z, and of order 10% for $m_{P^0} \sim m_Z$.

Finally, we discussed how the high-precision $gg \to P^0 \to \gamma\gamma$ LHC measurement can be combined with the precision $\mu^+\mu^-$ collider measurement of $\Gamma_{P^0}^{\rm tot}$ to determine N_{TC}, and how the values of N_{TC} and $\Gamma_{P^0}^{\rm tot}$ can be combined with the precision $\mu^+\mu^-$ measurements of various channel rates to determine (up to a discrete set of ambiguities) the six mass parameters of the effective low-energy Yukawa Lagrangian that determine $T_3 = -1/2$ fermion masses and their couplings to the P^0, and how all the above can, in turn, be used to determine the cut-off scale Λ from the measured value of m_{P^0} under the assumption that mass-squared contribution coming from one-loop diagrams involving SM fermions dominate over technileptoquark mass-squared contributions. We found that the accuracies for the measurements would very probably be systematics dominated. For systematic errors (associated with separation of different final states, *e.g.* using b-tagging, and with absolute rate normalization) in the expected $\sim$ 10% range, all the above parameters could then be determined within $\sim$ 15% overall systematic error, with somewhat smaller statistical error. Finally, we noted that the very accurate $\gamma\gamma$-collider measurement of the rate for $\gamma\gamma \to P^0 \to b\bar{b}$ would allow us to check the consistency of the formulae for the $\gamma\gamma P^0$ and ggP^0 anomalous couplings. Thus, we conclude that a detailed study of the lightest PNGB state of the broad class of technicolor models discussed here is possible and will reveal a great deal about the low-energy effective Lagrangian for the model. As described, a muon collider would play an absolutely essential role in such a study.

Acknowledgements

The research of RC, SDC, DD, AD and RG has been carried out within the Program Human Capital and Mobility: "Tests of electroweak symmetry breaking and future European colliders", CHRXCT94/0579 and No. OFES 950200. AD acknowledges support of a "Marie Curie" TMR research fellowship of the European Commission under contract No. ERBFMBICT960965. RC would like to thank Prof. J.P. Eckman for the kind hospitality of the physics department of the University of Geneva. JFG is supported by the U.S. Department of Energy under grant No. DE-FG03-91ER40674 and by the U.C. Davis Institute for High Energy Physics. JFG would also like to thank the University of Florence and the INFN for support and hospitality during the completion of this project. JFG thanks T. Barklow and H. Frisch for providing important details regarding detector parameters, H. Frisch and P. Wilson for details regarding the CDF RunI inclusive $\gamma\gamma$ analysis, and R.S. Chivukula and C. Hill for valuable theoretical discussions. RG thanks M. Mangano for information on the CDF $\gamma\gamma$ study.

References

[1] A. B. Bég, H. D. Politzer and P. Ramond, *Phys. Rev. Lett.* **43** (1979) 170; S. Dimopoulos, *Nucl. Phys.* **B168** (1980) 69; J. Ellis, M. K. Gaillard, D. V. Nanopoulos and P. Sikivie, *Nucl. Phys.* **B182** (1981) 529; R.S. Chivukula, M. Golden and E.H. Simmons, *Nucl. Phys.* **B363** (1991) 83.

[2] S. Dimopoulos, S. Raby and G. L. Kane, *Nucl. Phys.* **B182** (1981) 77.

[3] E. Eichten, I. Hinchliffe, K. Lane and C. Quigg, *Rev. Mod. Phys.* **56** (1984) 579; E. Eichten, I. Hinchliffe, K. Lane and C. Quigg, *Phys. Rev.* **D34** (1986) 1547.

[4] R. Casalbuoni, P. Chiappetta, S. De Curtis, A. Deandrea, D. Dominici, and R. Gatto, *Z. Phys.* **C65** (1995) 327.

[5] R. S. Chivukula, R. Rosenfeld, E. H. Simmons and J. Terning, hep-ph/9503202, in *Electroweak Symmetry Breaking and Beyond the Standard Model*, ed. by T. Barklow, et al. (World Scientific), p. 352.

[6] E. Eichten and K. Lane, *Phys. Lett.* **B388** (1996) 803.

[7] E. Eichten and K. Lane, *Proceedings of Snowmass 96: New Direction for High-Energy Physics*, June 25 – July 12, 1996, Snowmass, CO, eds. D. Cassel. L. Gennari and R. Siemann, p 1001, and references therein. See also, K. Lane, hep-ph/9605257.

[8] E. Eichten, K. Lane and J. Womersley, *Phys. Lett.* **B405** (1997) 305.

[9] V. Lubicz and P. Santorelli, *Nucl. Phys.* **B460** (1996) 3.

[10] R.S. Chivukula, hep-ph/9803219.

[11] P. Bhat and E. Eichten, FERMILAB-CONF-98/072.

[12] S. Weinberg, *Phys. Rev.* **13** (1976) 974; *Phys. Rev.* **19** (1979) 1277; L. Susskind, *Phys. Rev.* **20** (1979) 2619.

[13] For a review, see E. Farhi and L. Susskind, *Phys. Rep.* **74** (1981) 277.

[14] C.T. Hill, *Phys. Lett.* **B345** (1995) 483; K. Lane and E. Eichten, *Phys. Lett.* **B352** (1995) 382.

[15] B. Holdom, *Phys. Lett.* **B105** (1985) 301.

[16] K. Yamawaki, M. Bando and K. Matumoto, *Phys. Rev. Lett.* **56** (1986) 1335.

[17] T. Appelquist, D. Karabali and L.C.R. Wijewardhana, *Phys. Rev. Lett.* **57** (1986) 957; T. Appelquist and L.C.R. Wijewardhana, *Phys. Rev.* **D35** (1987) 774; *Phys. Rev.* **D36** (1987) 568.

[18] B. Holdom and J. Terning, *Phys. Lett.* **B247** (1990) 88. M. Golden and L. Randall, *Nucl. Phys.* **B361** (1991) 3; M. Peskin and T. Takeuchi, *Phys. Rev. Lett.* **65** (1990) 964; *Phys. Rev.* **D46** (1992) 381.

[19] M. Luty and R. Sundrum, hep-ph/9209255; S. Fleming and I. Maksymyk, *Phys. Rev.* **D53** (1996) 2781.

[20] T. Appelquist, J. Terning and L.C.R. Wijewhardhana, *Phys. Rev. Lett.* **79** (1997) 2767.

[21] R. Casalbuoni, S. De Curtis, N. Di Bartolomeo, D. Dominici, F. Feruglio and R. Gatto, *Phys. Lett.* **B285** (1992) 103.

[22] S. Coleman, J. Wess and B. Zumino, *Phys. Rev.* **D177** (1969) 2239; C. Callan, S. Coleman, J. Wess and B. Zumino, *Phys. Rev.* **D177** (1969) 2247.

[23] S. Chadha and M.E. Peskin, *Nucl. Phys.* **185** (1981) 61; *Nucl. Phys.* **187** (1981) 541.

[24] R. Renken and M.E. Peskin, *Nucl. Phys.* **B211** (1983) 93.

[25] S. Weinberg, *Physica* **96A** (1979) 327.

[26] For a recent pedagogical review that includes a discussion of this point, see A. Pich, hep-ph/9806303, especially the material on p. 46.

[27] R. Casalbuoni, S. De Curtis, A. Deandrea, D. Dominici, R. Gatto and J.F. Gunion, hep-ph/9801243, Contribution to the Proceedings of the Workshop on Physics at the First Muon Collider and at the Front End of a Muon Collider, Fermilab, Nov. 1997.

[28] A. Manohar and L. Randall, *Phys. Lett.* **B246** (1990) 537; L. Randall and E. H. Simmons, *Nucl. Phys.* **B380** (1992) 3.

[29] ATLAS Technical Proposal, CERN/LHCC/94-43, LHCC/P2.

[30] CMS Technical Proposal, CERN/LHCC 94-38, LHCC/P1.

[31] J.F. Gunion, G.L. Kane and J. Wudka, *Nucl. Phys.* **B299** (1988) 231; D.A. Dicus and S.D. Willenbrock, *Phys. Rev.* **D37** (1988) 1801.

[32] H. Frisch, private communication on behalf of the CDF collaboration.

[33] H. Baer and J.F. Owens, *Phys. Lett.* **205B** (1988) 377; E.W.N. Glover and A.G. Morgan, *Phys. Lett.* **B334** (1994) 208.

[34] ALEPH Collaboration (D. Buskulic *et al.*), *Z. Phys.* **C69** (1996) 365; CDF Collaboration (F. Abe *et al.*), *Phys. Rev. Lett.* **73** (1994) 2662.

[35] P. J. Wilson, for the CDF Collaboration, paper 675, submitted to *ICHEP 98*, Vancouver, BC, July 1998.

[36] CDF Collaboration (F. Abe *et al.*), hep-ex/9806034.

[37] B. King, contribution to the Proceedings of the Workshop on Physics at the First Muon Collider and at the Front End of a Muon Collider, Fermilab, Nov. 1997.

[38] T. Barklow, private communication, suggests that this might be possible.

[39] J.F. Gunion and H.E. Haber, *Phys. Rev.* **D48** (1993) 5109.

[40] D.L. Borden, D.A. Bauer, and D.O. Caldwell, *Phys. Rev.* **D48** (1993) 4018.

[41] T. Ohgaki *et al.*, *Int. J. Mod. Phys.* **A13** (1998) 2411; *Phys. Rev.* **D56** (1997) 1723.

[42] An early brief discussion of s-channel production of a vector technicolor resonance appeared in V. Barger, M. Berger, J.F. Gunion and T. Han, *Nucl. Phys. B (Proc. Suppl.)* **51A** (1996) 13. Other recent studies of both vector and scalar resonances, appear in: K. Lane, hep-ph/9801385; E. Eichten, K. Lane and J. Womersley, *Phys. Rev. Lett.* **80** (1998) 5489.

[43] G. Jikia and A. Tkabladze, *Phys. Rev.* **D54** (1996) 2030.

[44] R. Raja, contribution to the Proceedings of the Workshop on Physics at the First Muon Collider and at the Front End of a Muon Collider, Fermilab, Nov. 1997.

[45] V. Barger, M. Berger, J. Gunion and T. Han, *Phys. Rev. Lett.* **75** (1995) 1462; *Phys. Rep.* **286** (1997) 1.

[46] These are the current best estimates of R. Palmer, private communication.